Discover Applied Sciences

REVIEW Open Access

A comprehensive review of photocatalytic hydrogen evolution incorporating mechanisms and key parameters accompanying future outlook

Shaiza Asif[1], Khairul Anwar Mohamad Said[1,2*], Nadeem A. Khan[3], Imtiyaz Akbar Najar[1], Md Rezaur Rahman[1] and Kelvin Kuok King Kuok[4]

*Correspondence:
Khairul Anwar Mohamad Said
mskanwar@unimas.my
[1]Faculty of Engineering, University Malaysia Sarawak, 94300 Kota Samarahan, Malaysia
[2]Hydrogen Production, Techno-Economic & Sustainability (HPTeS), University Malaysia Sarawak, Sarawak 94300, Kota Samarahan, Malaysia
[3]Civil Engineering Department, College of Engineering, King Khalid University, Abha 61421, Saudi Arabia
[4]Faculty of Engineering, Swinburne University of Technology, Kuching, Malaysia

Abstract
The growing demand for sustainable and carbon-neutral energy carriers has intensified interest in hydrogen production via solar-driven photocatalysis. Despite extensive research on photocatalytic water splitting, practical implementation remains limited by low efficiency, stability issues, and the complexity of real-water matrices, particularly seawater. Unlike existing reviews that primarily emphasize catalyst design, this review uniquely integrates reaction parameters with water-source-specific behavior to provide a comprehensive understanding of photocatalytic hydrogen evolution. Key operational variables including water type, synthesis method, pH, temperature, light source, dissolved oxygen, and catalyst loading are systematically analyzed in relation to performance trends. A bibliometric analysis reveals rapid global growth in this field, dominated by China, India, and the United States, while highlighting underrepresentation in regions such as Malaysia. The parametric analysis identifies seawater salinity, ion interference, and operational conditions as critical bottlenecks limiting hydrogen yield and catalyst durability. By consolidating mechanistic insights, parameter-dependent effects, and bibliometric trends, this review outlines targeted research directions and provides a roadmap toward efficient, scalable, and seawater-compatible photocatalytic hydrogen production.

Keywords Seawater splitting, Hydrogen evolution, Oxygen evolution, Photocatalysis, Synthesis

1 Introduction

Energy production advanced at an extraordinary scale in the twentieth century, primarily due to the reliance on coal [1, 2], crude oil [2] and natural gas [3]. These resources fueled the expansion of industry, allowed for the transportation of goods around the world, and improved the standards of living in ways never seen before in human history. Yet the same resources are now on the basis of our environmental and social crises

today. The burning of fossil fuels has released massive amounts of greenhouse gases that have been responsible for global warming, ocean acidification, and extreme weather proceedings [4]. Air pollution from fossil consumption causes millions of premature deaths each year and extraction industries for fossil fuel cause environment loss and ecological damage [5]. Entering the twenty-first century, it has increasingly come to light that the current fossil-based energy paradigm cannot be maintained, either environmentally or economically [6].This recognition has shifted the focus of international attention to search for clean alternatives to the combustion of fossil fuels, and Hydrogen now is gaining momentum as a candidate fuel in the search for these clean alternatives [7].

Hydrogen is widely held to be a diverse energy carrier free of carbon with potential to revolutionize the world energy landscape [8]. It has by far the highest gravimetric energy density of any known fuel and produces only water when used inside fuel cells or during combustion processes. Its flexibility means it can be included in deployment across different sectors, if it also provides electricity via technologies such as proton exchange membrane and solid oxide fuel cells, used as a chemical feedstock in manufacturing ammonia and oil or as a clean fuel in the heavy transport and aviation sectors. Hydrogen also is seen as critical to decarbonizing sectors such as steelmaking or cement that cannot be easily electrified [9]. Strategic roadmaps prepared by the European Union, Japan, South Korea, and the United States predict a significant role for hydrogen in energy transition policies by mid-century [10]. However, the realization of a global hydrogen economy alters the attention on how hydrogen production is achieved, which raises a complex array of technologies that hold great promise, but also immediate critical challenges.

Currently, hydrogen production is primarily based on pathways relying on fossil sources. Approximately 95% of the global hydrogen supply is currently produced through steam methane reforming (SMR) and coal gasification, processes that are associated with substantial carbon dioxide emissions. To mitigate the environmental impact of these conventional hydrogen production routes, carbon capture and storage (CCS) technologies are being actively investigated. However, the implementation of CCS systems introduces additional economic costs and operational complexity, which remain significant challenges for large-scale deployment. Water electrolysis on the beach fueled by renewable power is a cleaner alternative and is at the heart of the concept of "green hydrogen" [11]. The high capital costs associated with electrolyzers, combined with the intermittency of renewable energy sources, currently render this approach economically uncompetitive. Alternative pathways, including thermochemical cycles and biomass gasification, are also under investigation; however, each faces limitations related to efficiency, cost, or scalability. These constraints underscore the need for innovative hydrogen production technologies capable of operating sustainably and economically at large scale.

One very promising route, overcoming many of these issues, is photocatalytic water splitting, in which the large capture of solar energy directly drives hydrogen production. Photocatalysis is a process in which semiconductors absorb photons and generate electron-hole pairs that can be used for generating redox reactions [12]. When used as a water splitting application, photogenerated electrons reduce protons to produce hydrogen, while holes oxidize water to produce oxygen. The concept was introduced by Fujishima and Honda in 1972 using titanium dioxide electrodes and kicked off decades

of research into alternative materials and system designs [13]. Photocatalysis has various attractive features including direct input of sunlight as energy, mild conditions in terms of temperature and pressure, and theoretically, feedstock is water. Unlike electrolysis, which requires external infrastructure for electricity use, photocatalysis combines the processes of capture from the sun and chemical conversion within a unified system, which increases the possibility of decentralized hydrogen production in areas with abundant sun exposure [14–16].

Over the past decade, research on hydrogen production through photocatalysis has expanded rapidly, with an estimated 10,000–15,000 studies reported in the literature stated below in Fig. 1 for Past decade publication on hydrogen production and photocatalysis. Among these, a significant amount, approximately 4,000–5,000 papers, focus on strategies such as catalyst doping, heterojunction construction, and defect engineering to enhance charge separation and exciton utilization. Efforts on tailoring crystalline structures and morphology account for another 1,500–2,000 studies, reflecting strong interest in improving stability and conductivity. More recently, the concept of electron storage and "dark photocatalysis" has emerged as a fast-growing subfield, with 400–600 publications since 2018. In terms of applications, hydrogen evolution dominates the research landscape, representing 60–70% of reports, while CO_2 reduction and environmental remediation contribute about 15–20% and 15%, respectively; organic synthesis remains less explored, but interest is rising. Publication activity has accelerated sharply, from fewer than 100 studies per year before 2010 to more than 2,000 annually by 2023–2024, underscoring the intense and expanding global effort toward advancing photocatalysis for sustainable energy and environmental applications.

According to Scopus documents survey on photocatalysis and hydrogen production Fig. 2 reveals a sharp geographical Contrarywise document publication, with China contributing 6000 documents, followed at a distance by India, the United States, and other

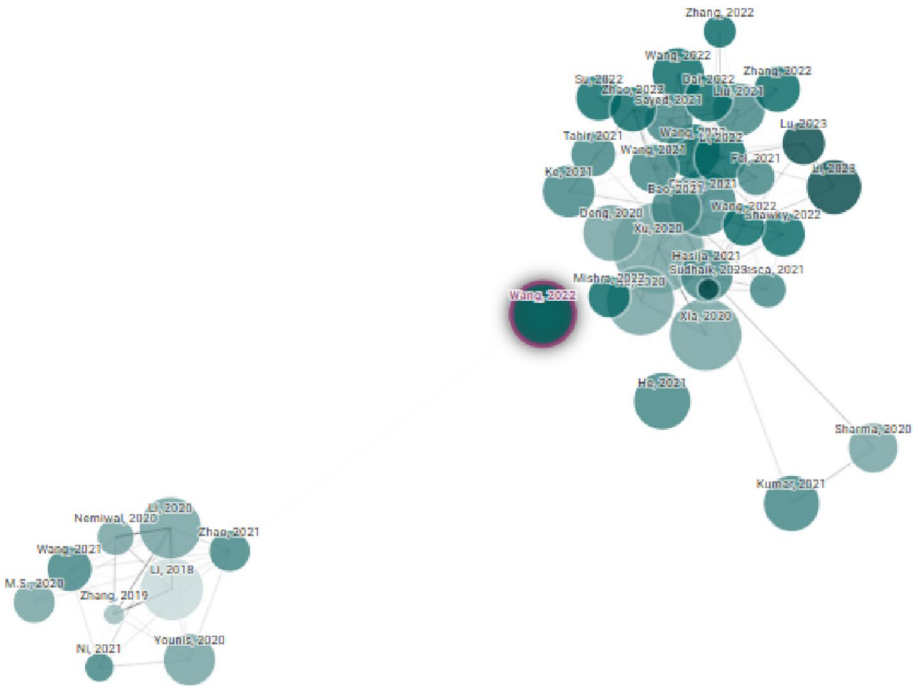

Fig. 1 Past decade publication on hydrogen production and photocatalysis

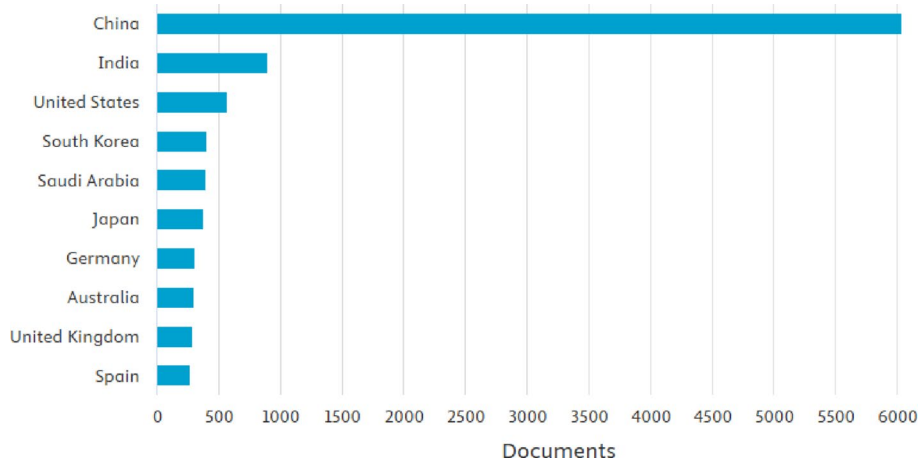

Fig. 2 Contrarywise document publication

active nations including South Korea, Japan, and Germany. Malaysia remains underrepresented in this rapidly advancing field, reflecting a critical gap in research visibility and impact.

Qu et al. [17] disclosed N-rich covalent organic framework (COF), ultrafine Ru comprising 1.3 nm nanoclusters and single atoms embedded in porous N-doped carbon was synthesized as an effective and stable electrocatalyst for both acidic and alkaline HER, exhibiting much higher mass activity than commercial Pt/C. The excellent HER performance arises from the abundant heteroatoms, strong Ru–N metal substrate interactions, and the large, porous surface area, which collectively enable low-content Ru (6.60 wt%) to perform efficiently. Experiments show that Ru single atoms and nanoclusters play complementary roles: single atoms facilitate water dissociation, nanoclusters promote H desorption, and hydrogen transfer occurs between them. The combination of a simple synthesis, ultralow Ru content, and the absence of template agents makes this catalyst cost-effective and promising for practical applications [17].

Yakub et al. [18] revealed Copper oxide supported on biochar offers a sustainable alternative to non-renewable catalyst supports for NO reduction, although it may suffer from low nitrogen selectivity and carbon combustion. Bimetallic catalysis is a proven approach to enhance catalytic performance. Accordingly, this study investigates carbon-supported copper oxides for selective NO reduction using hydrogen through the co-impregnation of iron or manganese. The catalysts were prepared by sequential incipient wetness impregnation, with copper oxide impregnated and calcined prior to the addition of the secondary metal. Iron–copper catalysts exhibited a 20% increase in nitrogen selectivity (approaching 100%) at 200 °C and a 20% reduction in carbon combustion at 300 °C, attributed to synergistic effects related to changes in elemental composition, acidity, and redox properties [18].

Reased et al. [19] review summarizes the advances made in the development of nanocomposite membranes and provides examples of how various nanostructures of materials (zero-dimensional, one-dimensional, two-dimensional, and three-dimensional) impact interactions with polymer matrices to enhance the properties of the membrane. The review discusses applications for these types of membranes in Reverse Osmosis, Nanofiltration, Ultrafiltration, Membrane Distillation and Treatment of Wastewater

Pollutants. The examples provided include both research studies and commercial examples of Thin Film Nanocomposite (TFN) membranes [19].

Despite this rapid progress, a critical gap remains in translating laboratory-scale photocatalytic hydrogen production into stable, scalable, and efficient systems for real-world conditions such as photocatalytic water splitting. To address process challenges, require a comprehensive parametric study guide for the rational design of practical photocatalytic systems. To establish a deeper mechanistic understanding considering parameters such as type of water, synthesis method, pH, temperature, light source, dissolved oxygen, and catalyst loading. To support the rational design of practical systems challenges and future perspective of photocatalytic hydrogen production are outlined in a dedicated section of this review.

2 Photocatalytic water splitting

2.1 Basic principles of water splitting

Photocatalytic water splitting is the process of utilizing photocatalysis to separate water (H_2O) into hydrogen (H_2) and oxygen (O_2). The inputs are light energy photons, water, and one or more catalysts. The procedure is modelled after the photosynthesis process, which uses water and carbon dioxide to produce oxygen and carbohydrates. Solar-powered water splitting is not yet commercially available [20]. In photocatalytic water splitting, photocatalyst particles are either dispersed directly within the aqueous medium or immobilized on a supporting substrate, in contrast to photoelectrochemical cells, which rely on the assembly of structured photoelectrodes [21]. The photoinduced electrons and holes participate in the reduction and oxidation of adsorbed water (H_2O) molecules, respectively, as these species interact with the catalyst surface [22]. To calculate the total efficiency of photocatalytic splitting of water used for production of (H_2), each step is crucial, as illustrated in Fig. 3 (a). Factors such as charge separation, charge transit, surface adsorption capacity, light harvesting, affect the quantum efficiency of photocatalysis.

Therefore, the present focus of new research is on designing photocatalysts to engineer the needed qualities. Either photocatalysis (PC) or photoelectrolysis (PEC) can be used to divide water using solar energy . The primary distinction between the two methods is the additional electrical energy that PEC requires in addition to photon energy. Modern

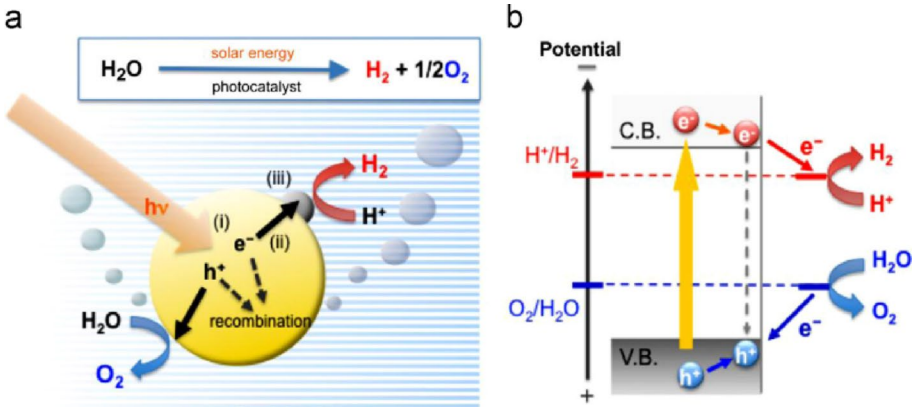

Fig. 3 Diagrammatic representation of water separating from semiconductors photocatalytic process. Reprinted from Yakubu Mohammed et al., "Hydrogen production via photocatalytic water splitting using spinel ferrite-based photocatalysts: Recent and future perspectives," Next Energy, 4, 100,145 (2024), licensed under CC BY 4.0 [28]

photoelectrochemical systems claim to have 2–3% sun-to-hydrogen conversion (STH) efficiency. Because photocatalytic devices have a smaller capacity for light harvesting, their STH efficiency can be as low as 0.1% [23, 24]. Water utilizing photocatalysts to split into oxygen and hydrogen is shown schematically. Three important processes engage in photocatalysis on semiconductor particles:

Step 1: The photocatalytic process begins with the activation of electron-hole pairs, triggered by photons with energy equal to or greater than the semiconductor's band-gap energy (Eg). Simply put, when electrons (e^-) in the valence band of the semiconductor get excited, they move to the conduction band, leaving behind holes (h^+) in the valence band, as shown in Fig. 3(a). To maximize the absorption of visible light photons, it's ideal to use a photocatalyst with a narrower band gap.

Step 2: Second stage shows how photogenerated holes and electrons can be separated. However, when most charge carriers undergo recombination, the number of energized charge carriers drops. This stage produces heat or phonons. Both holes and electrons can participate in a variety of surface chemical reactions by combining them. Photogenerated electrons are commonly regarded as reductants that can be used to reduce few heavy metal ions directly. Due to their considerable oxidizability, the separated holes can also directly engage in the oxidative breakdown process. This is the leading way that hydroxyl radicals (OH) are produced, or they can interact with a water molecule or a hydroxyl ion (OH^-).

Step 3: The third stage is the surface chemical reaction. Surface chemical interactions occur between carriers and various substances, such as H_2O. Additionally, electrons and holes can recombine without any chemical reactions. For water splitting using a heterogeneous semiconductor photocatalyst, the lower edge of the conduction band must be positioned at a more negative potential than the water reduction potential. At the same time, as illustrated in Fig. 3(b), the upper edge of the valence band must be positioned at a more positive potential than the water oxidation potential. Figure 3 shows the diagrammatic representation of several steps involved in the production of hydrogen through photocatalysis. These include the semiconductor photocatalyst's absorption of light, the creation of ecstatic carriers of charge (holes and electrons), their process known as recombination, the holes, and electrons migration, trapping of charge carriers and the transformation of these charge carriers to H_2O or other molecules [25, 26]. The overall hydrogen production in the photocatalyst setup is impacted by each of these phases. Hydrogen production amount depends on the quantity of excited electrons available to reduce water at the photocatalyst-water interface [27]. Charge carrier deactivation through bulk and surface recombination is detrimental to photocatalytic water splitting, as recombination processes dissipate energy in the form of phonons or radiative emissions, thereby reducing the population of active electron hole pairs. Consequently, efficient charge separation and rapid charge carrier transport, which suppress both bulk and surface recombination, are essential for enhancing photocatalytic hydrogen production via water splitting.

2.2 Hydrogen production photocatalytic process

The overall water splitting reaction (OWR) of a photocatalytic water splitting reaction is comprised of up of the hydrogen evolution reaction (HER) and the oxygen evolution

reaction (OER), two half-reactions. Figure 4 highlights the reaction involved in water splitting.

$$\mathrm{HER} : 4\mathrm{H}^{+} + 4\mathrm{e}^{-} \rightarrow 2\mathrm{H}_2 \tag{1}$$

$$\mathrm{OER} : 2\mathrm{H}_2\mathrm{O} \rightarrow 4\mathrm{H}^{+} + 4\mathrm{e}^{-} + \mathrm{O}_2 \tag{2}$$

$$\mathrm{OWR} : 2\mathrm{H}_2\mathrm{O} \rightarrow 2\mathrm{H}_2 + \mathrm{O}_2 \tag{3}$$

When an intense photon is absorbed and used to generate and separate charge carriers, within the valence band (V_b) the left holes begin to break water molecules into proton and oxygen gas, as shown in Eq. (2). According to Eq. (1), these protons engage with the free electrons in their conduction band (C_b), resulting in required H_2 gas. To achieve efficient and economic H_2 production, the photocatalyst must satisfy the varies fundamental specifications:

1. In a water splitting process the bandgap determines efficiency names as solar to hydrogen (STH) [26]. Therefore, bandgap of photocatalyst must be sufficiently low (1.23 eV < Eg< 3.0 eV) for utilization of visible light lying in solar spectrum [27].
2. V_b must be more positive than the water redox potential or oxidation water potential (1.23 V vs. NHE at pH = 0).In comparison, C_b must be negative (at least 0 V vs. NHE at pH = 0) than oxidation water potential [29].
3. The type of photocatalyst for the water splitting process must be stable and resistant towards chemical corrosion and photocorrosion [30].
4. Additional specifications involve cheap fabrication cost, scalability, non-toxicity, quick and effective charge transfer, vast surface reaction sites and recyclability/reusability [31].

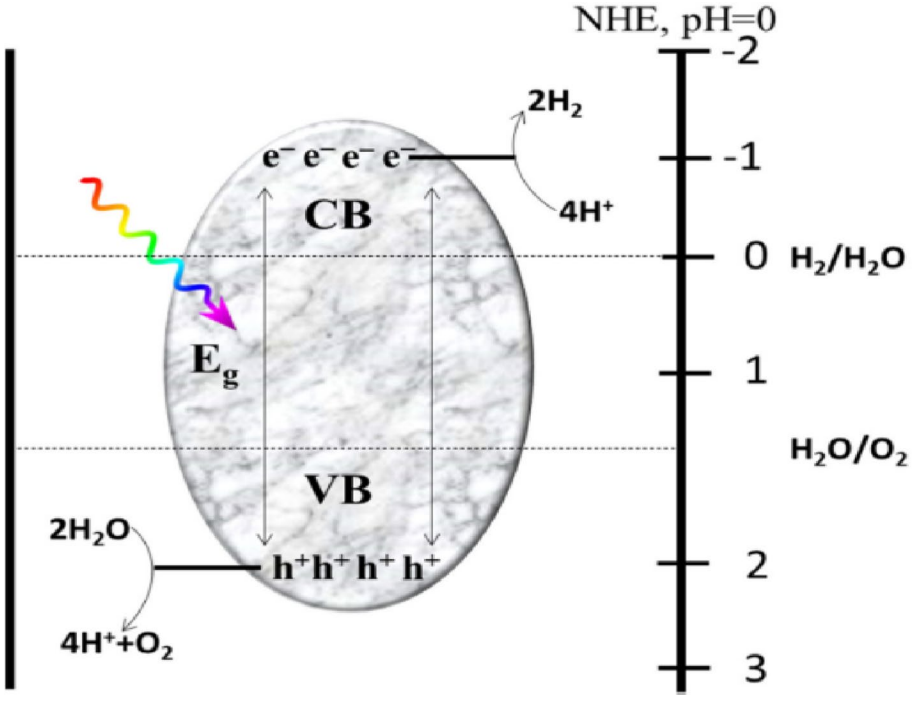

Fig. 4 Reaction involved in water splitting [25]

2.3 Evolutionary assessment of photocatalytic water splitting

To allow for meaningful comparisons between different photocatalysts under identical experimental conditions, the rate of gas production (oxygen and hydrogen) is measured in units like μmol h^{-1}. The quantum yield, a component of the overall quantum yield observed in a homogeneous photochemical system, is an important metric for assessing the activity of photocatalytic molecules in water splitting. This applies to both hydrogen and oxygen production. s specified by Eqs. (4) and (5), respectively [32].

For H_2 evolution

$$\text{Quantum yield}\,(100\%) = \frac{2^{*}\text{No.of } H_2\text{molecules evolved}}{\text{No.of incident photons}}{*}10 \tag{4}$$

For O_2 evolution

$$\text{Quantum yield}\,(100\%) = \frac{2^{*}\text{No.of } O_2 \text{ molecules evolved}}{\text{No.of incident photons}}{*}100 \tag{5}$$

Under irradiation conditions, the efficiency of photochemical water-splitting catalysts is usually measured by how much gas they produce (in mol/h) per gram of catalyst. To calculate the apparent quantum efficiency (QE), you can use the formula $QE = 2[H_2]/I$, where *I* represents the photon flux (mol/s) hitting the reaction mixture, and $[H_2]$ is the amount of hydrogen gas generated. However, because not all the photons from the light source are absorbed but some just pass through the quantum yield often end up being lower than the overall quantum yield.

3 Factors affecting water splitting for H2 production

Key operational parameters have vital role in regulating photocatalytic hydrogen evolution H_2 production via photocatalytic water splitting process efficiency is influenced by many factors illustrated in Fig. 5. In this study, only synthesis method, pH, temperature, light source, dissolved oxygen and catalyst loading are discussed in detail.

Water resource whether ultrapure water, seawater, or wastewater plays a critical role in photocatalytic performance, as dissolved ions and organic matter can poison active sites, induce competing reactions, or, in some cases, facilitate adsorption processes. The synthesis method strongly influences the structural properties of photocatalyst, including surface area, crystallinity, and light absorption behavior, which in turn determine hydrogen production efficiency. These properties also affect surface charge states, proton availability for reduction reactions, and the overall stability of the catalyst surface. Temperature governs both charge-carrier transport and reaction kinetics; moderate heating can enhance photocatalytic activity, whereas excessive temperatures may promote charge recombination or catalyst degradation. Dissolved oxygen acts as a competing electron acceptor, thereby suppressing hydrogen evolution, while simultaneously providing insight into charge-recombination pathways. Finally, catalyst loading affects light absorption and the number of accessible active sites. Insufficient catalyst loading limits photon absorption, whereas excessive loading can lead to light scattering and shielding effects, both of which reduce overall efficiency. Collectively, these parameters determine whether a photocatalytic system is suitable for laboratory-scale studies or has the potential for scalable, practical implementation.

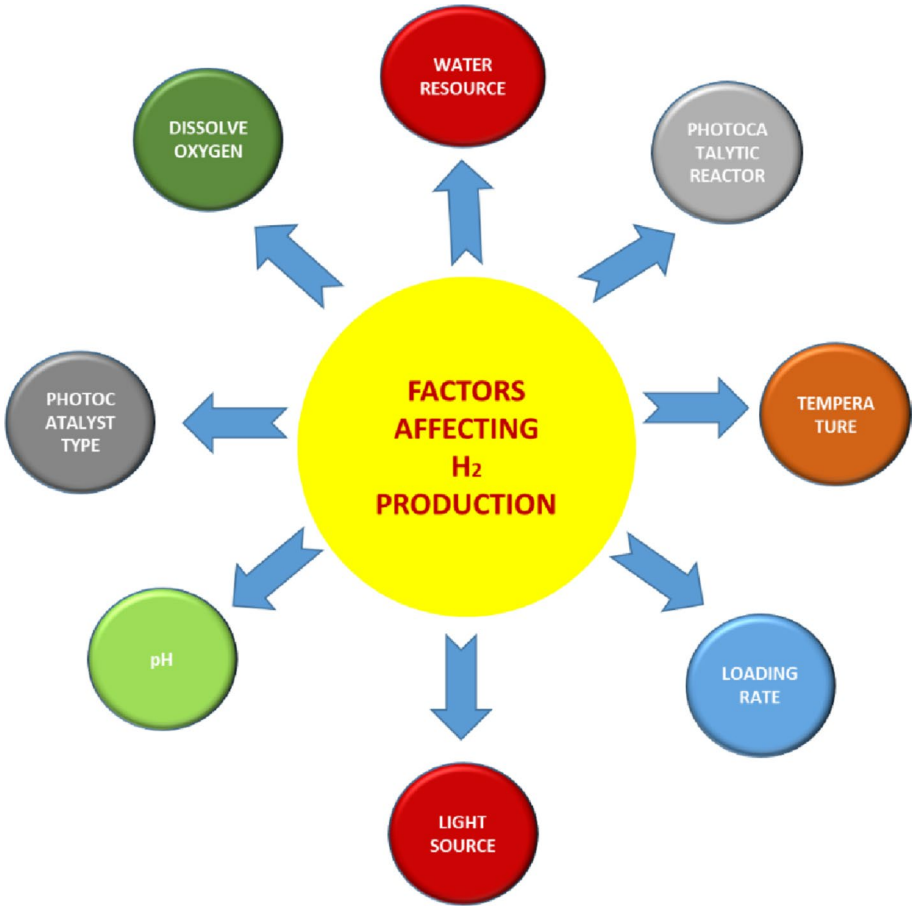

Fig. 5 Parameters affecting Photocatalytic H_2 production

3.1 Effect of synthesis method

3.1.1 Photothermal

One auspicious method of optimizing solar energy utilization to produce clean energy is photothermal-assisted photocatalytic hydrogen generation [33]. By increasing the local temperature and speeding up redox reactions and photoinduced carrier mobility, photothermal conversion [34] is an essential element that can significantly enhance catalytic processes [35]. To support this process Y. Shi et al. [36] created a composite photocatalyst for very effective $ZnIn_2S_4$ micro flower synthesis via core-shell Fe_3O_4@SiO_2 nanoparticle coating under photocatalytic water/seawater splitting with photothermal assistance. The greatest rates percentages of photocatalytic seawater/water splitting into hydrogen appeared much higher than those of pristine $ZnIn_2S_4$, reaching up to 1258.5 and 1108.5 $\mu mol \cdot g^{-1} \cdot h^{-1}$above Fe_3O_4@SiO_2/$ZnIn_2S_4$, respectively, by 11.9 and 14.7 times [37].

3.1.2 Sonophotocatalysis

Sonophotocatalysis was used to extract hydrogen and oxygen from water in an argon atmosphere, and the alternating irradiation approach was used to separate each product [38]. This technique is used for the decomposition of different contaminants, such as sonophotochemistry, which uses a variety of light frequencies in conjunction with ultrasonic waves to travel through fluid environments. Combining ultrasonic waves at

specific frequencies (25–800 kHz) with photocatalysis is considered one of the most effective ways to fully break down unstable pollutants. This approach enhances the overall efficiency of pollutant removal [36, 39].

The explanation for these effects is that increasing photoactivity through increased reactive surface area and separation of charges causes hydrogen bubbles to separate through the catalyst surface and increases the mass transfer of H_2 in the catalytic bulk surface. The idea of combining light and ultrasound to speed up the chemical reaction that produces hydrogen was addressed by Cotana et al. (2007) used a xenon lamp, which has a spectrum like sunlight, to simulate solar irradiation under different static pressures (1–3 atm). At the same time, they applied sonication at a frequency of 22.5 kHz with a power of 50 W. When power ultrasounds were coupled to light, it was found that hydrogen generation increased at a low static pressure of 1 atm.However, similarly to the photocatalysis technique, sonophotolysis for hydrogen production faces divergent results [40]. As Harada [41] assumed that the amount of H_2 produced is reduced by around 13.1% when ultrasound is added to the sonophotolysis of water. Nevertheless, sonophotolysis for the generation of hydrogen encounters conflicting outcomes, much like the sonophotocatalysis process. Additionally, the addition of ultrasound to the sonophotolysis process using water reduces the amount of hydrogen produced by around 13.1%, which is different from the study previously described [42].

3.1.3 Hydrothermal

The hydrothermal method is a top-down process where a chemical reaction between precursors in a solvent is driven by high temperature and pressure. Specifically, the reaction takes place in an enclosed system where the temperature exceeds the solvent's boiling point, creating a high-pressure, bubbling solution [43]. This method is environmentally friendly and yields materials with high uniformity, homogeneity, and fewer defects. Furthermore, it enables the production of particles or other targeted nanostructures with outstanding crystallinity, high purity, and precisely controlled properties [44].

The materials, which were created by a simple hydrothermal process, were used to separate deionized water, seawater, and artificial seawater under four hours of artificial sunlight. Virgin TiO_2 nanomaterials SnS_2/TiO_2, NiS_2/TiO_2, and CoS_2/TiO_2, were effectively used to create 48.11, 24.94, 15.04, and 2.78 $mmolg^{-1}$ of hydrogen, respectively [41]. Moreover, Z. Cheng et al. (2024) showed that converting the rutile/brookite type (1) hetero-phase junction into an anatase/brookite type (2) hetero-phase junction significantly improved the separation of photogenerated carriers. By designing a mesoporous structure, the number of active sites increased. Without using a sacrificial agent, the photocatalyst achieved an impressive hydrogen evolution activity of 6590 μmol g^{-1} h^{-1} in seawater, outperforming three commonly used TiO_2 materials: anatase/rutile mixed crystal (P25), brookite/rutile mixed crystal, and single-crystal nanoparticles [45].

Another study by J. Zhang et al. [14] showed the viability of the idea of using seawater instead of pure water through the application of Pt/anatase, Pt/rutile and Pt/brookite TiO_2 nanoparticles as photocatalysts. These nanoparticles have demonstrated favorable hydrogen production capability under the complete solar spectrum. It is noteworthy that brookite TiO_2 is more stable and efficient in the hydrogen production process than anatase and rutile TiO_2 due to its superior photoelectric characteristics and more appropriate band gap position. The maximum amount of hydrogen produced by brookite TiO_2

during full spectrum photocatalysis is 1476 μmol.g^{-1}.h^{-1}, which is higher than anatase and rutile TiO_2-based systems [46].

In another study, B.-J. Ng et al. [47] revealed for design of $ZnIn_2S_4$ (ZIS) atomic layers arranged in hexagonal shape in two dimensions (2D) with a focus on heteroatom P doping (ZIS-P) and H adsorption kinetics. This approach creates sacrificial agent-free photocatalytic HERs by altering intrinsic S active sites that can be used with both clean water and seawater. The optimal ZIS-P sample showed excellent photocatalytic water-splitting performance under visible light without relying on sacrificial chemicals. It achieved a hydrogen production rate of 1.68 μmol.g^{-1}.h^{-1}, in purified water and 1.54 μmol.g^{-1}.h^{-1}, in synthetic saltwater.

Lv et al. [48] demonstrated in his study that photocatalysts that exhibit high activity and resistance to photocorrosion were found to be crucial for the effective extraction of hydrogen energy from saltwater. This study describes the practical synthesis of through one-pot sulfidation and pyrolysis, graphene oxide formed a tight bond with high-index facets CD ZnS that had rich sulfur vacancies (Vs-CZS@GO). The careful defect, interface, and surface engineering gave Vs-CZS@GO high-index features with a considerable charge transfer behavior and a decreased ΔGH* value, which were validated by DFT calculation that allowed for efficient H_2 generation. In addition to improving essential site activity and carrier separation effectiveness, as well as the cooperative action of high-index facets, tightly linked interface, and sulfur vacancy also significantly increased the H_2 evolution rate and stability. As a result, in real seawater exposed to visible light, Vs-CZS@GO showed an extremely high rate of H_2-generation (23.2 mmol√g − 1√h − 1) which is up to 82% of that in pure water [49].

3.1.4 Doping

Substituting impurities or dopants for a small amount of ferrite spinel catalysts for photocatalysis is an effective approach for enhancing photocatalytic activity by introducing new reaction sites and optimizing energy bands [50]. These impurities or dopants might be metallic (gold, silver, platinum) or non-metal (C, N, S) etc. [51]. Additionally, by trapping photogenerated electrons, these dopants can lengthen their lifetime, reduce the recombination of carrier charges, and enhance photocatalytic activity [48].

By doping twin crystal $Zn_{0.5}Cd_{0.5}S$ with Bi, Yang et al. (2023) created a novel type for the first time, the structural features and properties of the Bi/twin crystal $Zn_{0.5}Cd_{0.5}S$ catalyst (Bi/ZCS) were thoroughly analyzed using XRD, XPS, TEM, Raman, and PL and how Bi doping affected the photocatalytic H_2 production efficiency of ZCS. By enhancing the separation of photogenerated carriers, the Bi/ZCS photocatalyst achieved a significant improvement in photocatalytic H_2 evolution. The optimized catalyst delivered an impressive apparent quantum efficiency of 31.5% at 420 nm and a high H_2 evolution rate of 1090 μmol.g^{-1}.h^{-1} (using 10 mg of catalyst), which was 4.16 times higher than that of ZCS alone [52].

Additionally, Y. He et al. demonstrated the viability of using an organic polymer porous triptycene function as an excellent catalyst for the conversion of solar energy using seawater. Here, the in-situ Suzuki reaction was used to coat a polymer triptycene on the surface of a $Cd\ Zn_{1-x}\ S$ nanorod to create TCP@CZS is a core-shell heterojunction. for photocatalytic H_2 synthesis by seawater/water splitting. TCP can be added to the proton reduction reaction to increase charge transfer, enrich the active site, and offer a large

surface area. Benefiting from it, optimum TCP@CZS showed that, in seawater in its natural state while being exposed to artificial sun light, Na_2S/Na_2SO_3 had an H_2 production rate of 93,800 μmol·g^{-1}·h^{-1}, which was 2.2 and 1.1 times greater than that of that in pure water using pure $CdZn_{0.4}$ S correspondingly [53]. For hydrogen evolution, Young et al. (2020) studied the impact of plasma irradiation on water photolysis was assessed. Silver (Ag) doping on the surface of TiO_2 decreased the bandgap and expanded the range of light absorption, on the TiO_2 surface Ag doping accelerated the process of hydrogen evolution [54].

According to A.E Giannakas et al., (2013) TiO_2 catalysts doped with nitrogen and co-doped with nitrogen and fluorine were synthesized using a sol–gel method. Ammonium chloride (NH_4Cl) and ammonium fluoride (NH_4F) were used as nitrogen and nitrogen–fluorine dopant precursors, respectively, with Ti: N and/or F molar ratios of 1:1, 1:2, and 1:3. The photocatalytic performance of the prepared catalysts was evaluated through the reduction of hexavalent chromium [Cr(VI)] in aqueous solutions containing oxalate ions. X-ray diffraction (XRD) analysis confirmed the formation of the anatase TiO_2 phase in all samples. UV–Vis diffuse reflectance spectroscopy (UV–Vis DRS) revealed a reduction in band-gap energy, with values of approximately 2.81 eV for N–F co-doped TiO_2 and 3.01 eV for N-doped TiO_2, indicating enhanced visible-light absorption, particularly for the N–F co-doped catalyst.The EPR results indicated: (i) the formation of NO centers, N• radicals, and $O_2•^-$ species; (ii) the presence of Ti^{3+} ions in the lattice of N–F co-doped TiO_2; and (iii) that the N• and Ti^{3+} species were photoactive, whereas the NO centers were not. The photocatalytic efficiency for Cr(VI) reduction in the presence of oxalate ions followed the order: TNF1 > TN1 > TNF2 > TN3 > TN2 > TNF3 [55].

3.1.5 Solvothermal

Metal oxides are typically prepared using this technique the term "solvothermal method" refers to the use of another solvent, such as ethanol, in place of water [44]. In an enclosed system heating a solvent and precursor related to that solvent at temperature above the boiling point of the solvent. At high temperature, the pressure increases, and the solvent's peculiar behavior under supercritical conditions all have an impact on the precursors, producing the desired substance [56].

To support this information, Sun et al. (2022) used the solvothermal approach to create S-scheme homojunction amorphous/high-crystalline g-C_3N_4 (HCCN/ACN), which can be used in water or marine conditions for photocatalytic H_2 generation [57]. The following explanations explain why the ACN/HCCN (6:4) s-scheme in saltwater 3.14×10^3 μmol·g^{-1}·h^{-1} and water 5.5×10^3 μmol·g^{-1}·h^{-1}, homojunction exhibits the highest photocatalytic H_2 evolution rate. In another study, Han et al. (2022) introduced a new amorphous FexP that was successfully produced and attached to the surface of $Mn_{0.3}$ $Cd_{0.7}$ S nanorods by a mild solvothermal method. FexP/$Mn_{0.3}Cd_{0.7}S_{-0.2}$ composite achieved 31,420 μmol.g^{-1}.h^{-1}, maximum H_2 generation, which is 766.34 times that of $Mn_{0.3}Cd_{0.7}$ S [58].

Ultrathin inorganic nanosheets have attracted increasing attention for photocatalytic CO_2 reduction due to their unique electronic structures and excellent charge transport properties. Zhu et al., (2025) revealed Selenium vacancy rich Bi_2Se_3 nanosheets with in situ formed bismuth metal clusters have been synthesized via a solvothermal route followed by hydrogen annealing, where surface selenium vacancies act as electron-trapping

and CO_2 adsorption sites, while bismuth clusters promote charge transfer and catalytic reactions. This dual-functional architecture enables unidirectional electron transfer along the topologically conductive surface, resulting in enhanced CO production. The optimized V-Bi_2Se_3–3 catalyst achieved a CO yield of approximately 130 μmolg^{-1}, significantly outperforming unannealed samples, demonstrating that defect engineering combined with in situ metal cluster formation is an effective strategy for enhancing photocatalytic CO_2 reduction performance [59]. In another study, the incorporation of isolated Co single atoms into ultrathin BiOCl nanosheets was shown to redistribute surface charge density, suppress electron–hole recombination, and enhance CO_2 adsorption and activation through Bi–O–C(=O)–Co coordination on the (001) facet, resulting in a CO formation rate of 183.9 μmol g^{-1} h^{-1} without cocatalysts or sacrificial agents [60].

3.1.6 Ball milling

Ball milling is a technique for crushing nanotubes into incredibly tiny particles. Localized high pressure is created during this process when the small, hard balls collide in a hidden container. Stainless steel, ceramic, and flint stones are typically utilized [61]. Mumtaz et al. (2024) designed a hybrid composite of bismuth sodium titanate ($Bi_{0.5}$ $Na_{0.5}TiO_3$) with superimposed Co_3O_4 functionalized RGO as reinforcement via z scheme. A 14.79% increase in H_2 production has been reported by the addition of reinforcement plus 5% RGO-Co_3O_4 H_2 production of (517 μmol/g^{-1} h^{-1}) has been reported. Moreover, using only photocatalysis, the production is 66 μmol.g^{-1}.h^{-1}, while in piezophotocatalysis, 109 μmol.g^{-1}.h^{-1} H_2 production has been detected [62].

An improvement of 1.8% in seawater and 50.4% in manure H_2 evolution has been reported. Guo et., (2023) synthesized a unique and effective H_2 production by Br-doped C, N-deficient CN (CNV-mCN-Br) photocatalyst using a ball-milling and calcining procedure. Theoretical computations and systematic characterization revealed that CNV-mCN-Br, in the presence of TEOA, demonstrated a fascinating photocatalytic H_2 evolution performance in both simulated seawater and water, with separated electron-hole distribution and corresponding H_2 rates of 22,210 and 34,410 μmol.g^{-1}.h^{-1}, over 1% Pt-loaded CNV-mCN-Br. This work offers a new and straightforward way to alter CN with significantly improved H_2 evolution photocatalytic performance [63].

3.1.7 Photochemical

Photochemistry is the study of chemical processes continued by light [64]. Photochemistry, in its broadest sense, is the study of chemical reactions initiated by the absorption of light [65]. In these processes, light provides the energy required to break chemical bonds or electronically excite molecules, creating pathways distinct from thermal reactions. The "thermal" reactions discussed thus far rely instead on exothermicity as their driving force, with reaction barriers being surmounted by the thermal energy of the reactants [65] Photochemical reactions are distinguished by their driving force: the absorption of light. In the atmospheric context, the Sun provides this light, and the atmosphere itself functions as a vast photochemical reactor. Solar radiation (visible and UV) excites atmospheric molecules, which can either undergo a change in reactivity or dissociate to produce reactive species such as atoms, radicals, and ions [66].

C. Cheng et al. (2022) revealed that Schottky barriers at the semiconductor/metal boundary lead to hole/electron separation, but they also restrict electron migration

surrounded by interface boundary. Here, they adjust Schottky barriers over $Mn_{0.3}Cd_{0.7}S$ (Ni/MCS-s) composites that are rich in Ni/S vacancies and were made using a photochemical and self-assembly process. In artificial seawater (3.5 weight% NaCl), the Ni/MCS-s heterostructures demonstrate better H_2 generation up to 164,100 $\mu mol \cdot g^{-1} \cdot h^{-1}$, which is 68 and 5 times greater than MCS-s and one weight% Pt/MCS-s, respectively [67].

3.1.8 Sol-gel

The widespread adoption of this method can be attributed to its capability to operate at ambient temperature, coupled with the straightforward incorporation of chemical doping. The underlying principle of this technique involves the hydrolysis of a precursor containing solution, resulting in the formation of suspended colloidal nanoparticles. During the subsequent condensation phase, these colloids interact to generate a gel-like matrix [68].Dholam et al. (2009) achieved the synthesis of Fe and Cr doped TiO_2 thin films using a combination of room temperature and sol-gel technique. These innovative photocatalysts were then evaluated for their ability to produce hydrogen under visible light. The findings revealed that the doped TiO_2 materials exhibited significantly enhanced activity compared to their undoped counterparts. This improvement was attributed to the presence of Cr and Fe, which effectively function as electron-trapping agents, thereby boosting the photocatalytic performance [70].

Onsuratoom et al. [69] aimed to examine how the composition of mesoporous TiO_2-ZrO_2 mixed oxide nanocrystals plays a key role in their ability to produce hydrogen from water splitting under UV light. These nanocrystals were made using a sol-gel method with a structure-directing surfactant. A TiO_2-ZrO_2 photocatalyst, with a TiO_2-to-ZrO_2 molar ratio of 93:7 and calcined at 500 °C, showed impressive photocatalytic hydrogen production. Adding 0.5 wt% silver (Ag) further boosted the photocatalytic activity of the TiO_2-ZrO_2 mixed oxide photocatalyst. The Table 1 highlights remarkable progress in photocatalytic water splitting, with hollow tubular g-C_3N_4 and TiO_2-rGO-Cu standing out as star performers, achieving hydrogen yields as high as 6782–8683 and 16.1×10^3 $\mu mol \cdot g^{-1} \cdot h^{-1}$, respectively. These materials excel due to their ability to absorb light efficiently, separate charges effectively, and leverage unique structural advantages. $ZnIn_2S_4$ based catalysts also show enormous potential, especially when enhanced with dopants or co-catalysts, delivering moderate to impressive yields ranging from 1.54 to 164.1×10^3 $\mu mol \cdot g^{-1} \cdot h^{-1}$. Despite these successes, hurdles remain, such as photo corrosion in materials like CdS, the excessive costs associated with using platinum (Pt) or reduced graphene oxide (rGO), and the scalability challenges posed by complex synthesis processes, as seen with hollow g-C_3N_4 [70].

The most widely used synthesis methods, like hydrothermal and solvothermal processes, are favored for producing high-quality crystalline materials, while newer techniques such as microwave-assisted synthesis and ball milling offer faster, more energy-efficient alternatives, though they still need refinement. Subsequent research should be on creating affordable, durable, and scalable photocatalysts. This could involve replacing expensive materials like Pt with more abundant, low-cost alternatives, improving the ability of catalysts to harness visible light, and designing advanced heterojunctions to boost charge separation. Additionally, fine-tuning reaction conditions such as optimizing pH and catalyst loading and scaling up production methods will be essential

for moving these technologies from the lab to real-world applications. By addressing these challenges, we can pave the way for sustainable hydrogen production using sunlight, bringing us closer to a cleaner energy future. The comparative summary is stated below in Table 1.

3.2 Water resource and photocatalysis

As oceans and seas encompass 96.5% of the planet's hydrosphere, seawater consequently serves as the most prevalent and voluminous natural source of aqueous electrolyte solutions [82]. Direct hydrogen production through the photo-induced seawater splitting technique is recently being viewed as a viable option for industrialization and clean water replacement. It's interesting to note that using solar-powered photocatalytic seawater splitting technologies has a lot of potential for sustainably producing hydrogen. This plan provides a workable way to get clean and renewable energy. Despite the recent research papers on photocatalysis reactions and methodologies, including light source, water/seawater, and photocatalyst engineering. Gaining essential understandings into the current state of development of photocatalytic seawater splitting to produce (H_2) is made easier with the help advantages of employing photocatalytic seawater splitting to produce hydrogen, there are still several difficulties and complications that must be

Table 1 Comparative summary of Synthesis Methods

Synthesis Method	Advantages	Limitations	Typical Performance Outcome
Hydrothermal	Produces well-crystallized ZnO, good control over morphology (nanorods and nanosheets)	Long reaction times, autoclave, scaleup limitations	**300–800 µmol H_2 g^{-1} h^{-1}** under UV/visible light due to improved crystallinity and charge separation [71], [72]
Solvothermal	Uniform high surface area nanostructures, improved graphene dispersion of organic solvent	Costly solvent requirement, Post annealing needed	**250–700 µmol H_2 g^{-1} h^{-1}**, strongly dependent on solvent type and well-developed ZnO–graphene interfacial contact [69], [73]
Ball Milling	Simple, low-cost, scalable, enhances graphene exfoliation	Possible crystallinity loss, limited morphology control, defect damage may occur	**300–600 µmol H_2 g^{-1} h^{-1}**; activity improves after annealing or metal doping [74], [75], [76]
Sonophotocatalysis	Excellent mixing via cavitation, prevents graphene agglomeration, strong interfacial contact	Energy-intensive, difficult to scale, may need post annealing	**140–1500 µmol H_2 g^{-1} h^{-1}** due to enhanced mass transfer and charge separation [77], [78]
Doping	Improved visible light absorption, extended carrier lifetime, synergistic with graphene	Overdoping causes recombination, noble metal cost	**600–3240** µmol H_2 g^{-1} h^{-1} depending on dopant type and loading
Photochemical	Simple, low temperature, good nucleation control, homogeneous composites	Low crystallinity without annealing, slow, sensitive to Light condition	**250–700 µmol H_2 g^{-1} h^{-1}** under UV or visible light irradiation, attributed to improved metal–semiconductor interfacial contact and reduced charge recombination [79], [80]
Sol–gel	Uniform precursor distribution, cost-effective, scalable	High temperature calcination required, graphene oxidation possibility	**200–1200 µmol H_2 g^{-1} h^{-1}** under UV or simulated solar light, mainly influenced by calcination temperature, crystallinity, and cocatalyst loading [81][81]

worked out. These consist of scalability, charge carrier dynamics low reactivity, light absorption, affordability, and photocatalyst stability and corrosion [83, 84].

The hydrogen evolution reaction (HER) mechanism resembles pure water splitting once the seawater-splitting process is considered. However, compared to pure water-splitting processes, it becomes more complex when inorganic salt ions are included, especially the primary constituents of cations and anions of NaCl due to reaction on the photocatalyst surface. It is important to understand that certain components containing ions such as K^+, Mg^{2+}, Ca^{2+} also exhibit advantageous thermodynamics and kinetic interactions in saltwater. However, due to their much lower concentrations than the prevalent Na^+ and Cl^- ions, these ions are frequently disregarded and not well investigated. During photocatalytic seawater splitting, competing reactions involving oxygen evolution reaction (OER) and chloride byproducts coincide [85]. Table 2 featured an extensive selection of water source information.

The studies summarized in Table 2 reveal clear performance trends across synthesis methods, reaction conditions, and water source. Hydrothermal and solvothermal methods consistently yield higher H_2 production, as these approaches promote better crystallinity, controlled morphology, and efficient heterojunction formation. Among all catalyst systems, sulfide-based photocatalysts (CdS, $ZnIn_2S_4$, Mn–Cd–S composites, Ni/MCS-s) exhibit the highest hydrogen yields due to strong visible-light absorption and enhanced charge separation. In contrast, oxide-based photocatalysts (TiO_2, $Na_2Ti_3O_7$, Bi-based oxides) generally show moderate activity unless coupled with co-catalysts or conductive materials such as Pt or rGO.Water source also influences performance. Artificial seawater often results in higher yields than natural seawater, likely due to fewer impurities and lower ion interference. High salinity and ionic strength lead to charge screening and competitive adsorption of ions such as Na^+, Cl^-, Mg^{2+}, and SO_4^{2-} on catalyst surfaces, while chloride ions may both inhibit water oxidation through hole scavenging and simultaneously generate reactive chlorine species that alter oxidation pathways. The slightly alkaline pH (7.8–8.3), reduced dissolved oxygen levels, natural organic matter, and turbidity further complicate charge transfer and photon absorption, collectively reducing hydrogen evolution efficiency compared to pure water Additionally, systems employing visible or full-spectrum light sources outperform UV-dependent configurations, highlighting the importance of designing catalysts with strong visible-light absorption

3.3 Effect of pH

According to earlier research, one of the most crucial elements affecting the rate of photocatalysis is pH for hydrogen production [94]. In photocatalysis, hydroxyl radicals (OH) perform an important part in conversion of organic contaminants to CO_2 and H_2O. A problem, though, is electron-hole recombination prior to surface engagement. The reason the effect of pH is difficult to examine is because of the various reasons states as:- (i) the pH effect relies on the specifications of the photocatalyst and substrate, and (ii) the pH of solution changes as the reaction progresses due to the constant production and consumption of hydroxide anions hydronium cations [95]. The distinct impacts of pH must first be identified so that one can kinetically predict how pH affects photocatalytic reactions. The suspension's pH significantly affects the characteristics of the photocatalyst, including surface charge [96], functional groups [97], and particle size distribution [98], In contrast, pH affects how the substrate dissociates [99] and interacts with the

catalyst surface [99]. From a mechanical perspective, pH influences the protons concentration that are converted to hydrogen molecules stated below in Table 2's reaction (j) [100, 101].

The two main reasons why pH affects the photocatalytic process one is adsorption of substrates on catalyst surface and other is particle agglomeration of photocatalyst. A point comes when particles carrying no surface charge and that point is called zero-point charge (pHzpc), then particles of TiO_2 starts to agglomerate [96, 97, 102]. At pH levels either higher or lower than pHzpc, TiO_2 particles have a negative or positive charge, respectively. Since at pHzpc, the interaction rejection necessary to keep catalyst particles stable in the solution is not there. As a result, TiO_2 clusters grow and assemble within a ± 30 mV zeta potential range [96]. The average TiO_2 particle size can be between 2 and 4 mm close to pHzpc, but it can drop to 300 nm at a pH that is far away from pHzpc [97].The ability of catalysts to absorb substrates, transition, and absorb light photons is influenced by the size of their particles. Furthermore, extremely vigorous agitation is necessary to maintain a stable suspension since the agglomerated catalyst tends to sediment, so it is important to keep in mind that this pHzpc of TiO_2 is unaffected by metal deposition [103–105]. Alcohol and other substrates having an OH group can adsorb on the catalyst surface through interactions of hydrogen bonding on the catalyst surface [106, 107]. Because it influences the substrate molecules affinity, the quantity of hydroxyl groups present on the catalyst surface is crucial. Equations (6) and (7), respectively, state that OH groups on the surface of catalyst dissolve under basic and acidic environments [97] :

$$\mathrm{TiOH_2^+} \leftrightarrow \mathrm{TiOH} + \mathrm{H^+} \tag{6}$$

$$\mathrm{TiOH} \leftrightarrow \mathrm{TiO^-} + \mathrm{H^+} \tag{7}$$

The dissociation constant of the above two equations is stated as: -

$$\mathrm{K_{a1}} = \frac{[\mathrm{TiOH}]\,[\mathrm{H^+}]}{[\mathrm{TiOH_2^+}]} \tag{8}$$

$$\mathrm{K_{a2}} = \frac{[\mathrm{TiO^-}]\,[\mathrm{H^+}]}{[\mathrm{TiOH}]} \tag{9}$$

Their values are stated as 2.4 and 8.0, respectively. Rearranging equations a and b to form a Henderson Hasselbalch equation that is related to pH of solution [108]: -

$$\mathrm{pH} = \mathrm{pK_{a1}} + \log_{10}\frac{[\mathrm{TiOH}]}{[\mathrm{TiOH_2^+}]} \tag{10}$$

$$\mathrm{pH} = \mathrm{pK_{a2}} + \log_{10}\frac{[\mathrm{TiO^-}]}{[\mathrm{TiOH}]} \tag{11}$$

When pH equals pKa, exactly half of the OH groups on the catalyst surface have dissociated, per Eqs. (10) and (11). Conversely, the hydroxyl groups of the substrate and those located on the TiO_2 surface form a hydrogen bond, which enables the substrate to adsorb on the catalyst surface. Consequently, when $pKa_1 < pH < pKa_2$, the alcohol often

Table 2 Water source for photocatalytic Hydrogen production

Water Resources	Synthesis Method	Reaction conditions	H_2 yield $\mu mol.g^{-1} h^{-1}$	Key Findings	Limitations	Future Implications	Refs.
Artificial & Natural Seawater	Hydrothermal	CdS = 50,100,1 50 mg L^{-1} Visible light 9 W, pH = 10.0 ± 0.2,	(21), (500)	Moderate yield under visible light, suitable for pH-controlled environments	Prone to photo corrosion, limited stability under prolonged irradiation	Develop protective coatings or doping to enhance stability	[86]
Seawater	Piezo photocatalysis (Ball milling)	$Bi_{0.5}Na_{0.5}TiO_3$/RGO-Co_3O_4 25 g ($Bi_{0.5}Na_{0.5}TiO_3$), 5%, 10%, and 15% (RGO-Co_3O_4)	(517)	Enhanced yield due to piezo-photocatalytic effect and improved charge separation	Complex synthesis, high cost of RGO, scalability challenges.	Explore cost-effective alternatives to RGO for large-scale applications	[62]
Water & Artificial Seawater	Photothermal Assisted photocatalysis (Solvothermal)	Fe_3O_4@SiO_2/ $ZnIn_2S_{4=}$25 mg Solar energy 300 W Xenon lamp,	(1258.5), (1108.5)	High yield due to heterojunction formation and efficient charge transfer	Requires high-energy light sources, limited visible light absorption	Optimize for visible light absorption and reduce energy requirements.	[37]
Artificial seawater, Natural Seawater, Deionized water	Sol-gel & Facile Hydrothermal	NiS_2/TiO_2, CoS_2/TiO_2, SnS_2/TiO_2, Virgin TiO_2, 10 wt %, Simulated solar irradiation	(49.89,39.50,10.05,15.10), (48.11,24.94, 15.04,2.78), (41.78,8.59, 6.52,1.86)	Facile synthesis, moderate yield, suitable for artificial seawater	Low yield compared to other composites, limited by charge recombination.	Improve charge separation through advanced heterojunction design	[87]
Artificial Seawater	Suspended photocatalysis	Brookite/ Anatase TiO_2 = 5 mg, Hg lamp	(6.59)	Simple catalyst system with low yield under UV light.	Poor visible light absorption, low efficiency under solar light.	Modify TiO_2 for visible light absorption or combine with other semiconductors.	[45]
Artificial Seawater	One-pot microwave-assisted synthesis	In_2S_3/In_2O_3 nanosheets = 2.5-20mM 5 W Blue-LED light (λ = 420 nm, Ph = 2.55, 7.65 8.62, 10.52	(618), (17.7), (267.7), (448.1)	High yield under low-intensity light, efficient charge separation	Limited scalability of microwave synthesis, stability issues under long-term use.	Scale up microwave synthesis and improve catalyst stability.	[88]
Natural Seawater & Artificial Seawater	Photocatalysis	CdS & Na_2S/Na2SO3 = 50 −150mgL^{-1} UV lamp, pH = 10.0 ± 0.2	(390), (270)	Moderate yield, suitable for natural seawater applications.	UV light dependency, photocorrosion, and limited stability.	Develop UV-resistant CdS-based catalysts for improved stability.	[86]

Table 2 (continued)

Water Resources	Synthesis Method	Reaction conditions	H_2 yield $\mu mol.g^{-1} h^{-1}$	Key Findings	Limitations	Future Implications	Refs.
Natural seawater, Artificial seawater, Distilled water	Hydrothermal	$Na_{0.5}Bi_{0.5}TiO_3/Na_{0.5}Bi_{4.5}Ti_4O_{15}$ (NBT/NBT_4) =100 mg, All spectrum light 300 W	(140)	Moderate yield with full-spectrum light utilization.	Complex synthesis, limited yield compared to other composites.	Simplify synthesis and enhance light absorption for higher yields.	[89]
Artificial Seawater	Facile Hydrothermal method (photocatalysis)	Bi-doped $Zn_{0.5}Cd_{0.5}S$ (Bi/ZCS) =10 mg, 300 W Xe lamp (λ ≥ 420 nm)	(1.2)	Doping improves light absorption, but yields remain low.	Low hydrogen yield, limited by charge recombination and stability issues.	Optimize doping levels and explore co-catalysts for enhanced performance.	[52]
Artificial Seawater	Hydrothermal & Doping method	$ZnIn_2S_4$-P (ZIS-P) =10 mg, 350 W Xe lamp (λ > 420 nm)	(1.54)	Moderate yield, doping enhances charge separation.	Limited scalability, high cost of doping materials.	Develop cost-effective doping strategies for scalable production.	[47]
Artificial Seawater	Hydrothermal & Dipping method	TiO_2-rGO-Cu=20 mg, Xenon light (λ = 250–780 nm)	(16,100)	High yield due to improved charge separation and light absorption.	High cost of rGO and Cu, complex synthesis process.	Explore alternative materials to replace rGO and Cu for cost reduction.	[90]
Artificial Seawater & Distilled water	Ball milling & calcination (Photocatalysis)	CNv-mCNBr,1%Pt-loaded 300 W Xe lamp (λ ≥ 420 nm)	(34.4), (22.21)	Moderate yield, Pt loading enhances catalytic activity.	High cost of Pt, limited scalability of ball milling.	Replace Pt with low-cost co-catalysts for large-scale applications.	[63]
Artificial Seawater	Hydrothermal	Brookite TiO_2,3.0 mg Pt/TiO_2 Solar spectrum (full)	(1476)	High yield with Pt loading, suitable for solar light.	High cost of Pt, limited scalability.	Replace Pt with earth-abundant co-catalysts for cost-effective production.	[46]
Artificial Seawater & water	Solvothermal	HCCN/ACN 6:4 S-scheme,300 W Xe lamp	(3,100), (5,500)	High yield due to S-scheme heterojunction.	Complex synthesis, high cost of materials.	Simplify synthesis and explore low-cost alternatives	[57]
Artificial Seawater	Hydrothermal	Z-scheme $Na_2Ti_3O_7$/Ag/CdS = 50Mg, 300 W Xe lamp (λ ≥ 420 nm)	(1,793)	High yield due to Z-scheme heterojunction	High cost of Ag, limited scalability.	Replace Ag with low-cost materials for large-scale applications.	[91]

Table 2 (continued)

Water Resources	Synthesis Method	Reaction conditions	H_2 yield $\mu mol.g^{-1} h^{-1}$	Key Findings	Limitations	Future Implications	Refs.
Natural seawater	One pot sulfidation (pyrolysis) & DFT	Vs-CZS@GO,300 W Xe lamp	(23.2)	Moderate yield, efficient charge separation.	Limited scalability, high cost of GO.	Explore cost-effective alternatives to GO.	[49]
Natural Seawater, Artificial seawater, Deionized water	Thermal treatments, Ionothermal & photo deposition method.	Pt/GaP-C_3N_4, 0.3PGC50 (0.3 wt% Pt-loaded and 50 wt% GaP) 300 W Xe lamp (Solar Simulated), Ph = 7.7,7.5	(46.5), (53.9), (65.5)	Moderate yield, Pt loading enhances catalytic activity. Suitable for solar light	High cost of Pt, limited scalability.	Replace Pt with low-cost co-catalysts for large-scale applications.	[92]
Artificial seawater & water	Hydrothermal	Hollow tubular g-C_3N_4 (TCN- 1.5) = 100mL, 300 W Xe lamp ($\lambda \geq 420$ nm)	(6,782), (8,683)	Extremely high yield due to hollow structure.	Complex synthesis, high cost.	Optimize synthesis for scalability, reduce production costs.	[93]
Artificial seawater	Photochemical Method & solvothermal	Ni/S$Mn_{0.3}Cd_{0.7}S$ (Ni/MCS-s) =100mL, 300 W Xe lamp ($\lambda \geq 420$ nm)	(164,100)	High yield, Ni doping improves charge separation.	High cost of Ni doping, limited stability under long-term irradiation.	Improve stability and explore low-cost doping alternatives.	[67]
Artificial seawater	Solvothermal	Pt/$Mn_{0.3}$ $Cd_{0.7}$ S = 500 mg, 300 W Xe lamp ($\lambda \geq 420$ nm)	(32,800)	High yield, Pt loading enhances catalytic activity.	High cost of Pt, limited scalability, and stability issues.	Replace Pt with earth-abundant co-catalysts for cost-effective production.	[58]
Natural Seawater	Hydrothermal	$Na_2Ti_3O_7$/CdS type II=50 mg, Visible-light irradiation	(184.8)	Moderate yield, type II heterojunction, improves charge separation.	Limited visible light absorption, stability issues under prolonged use.	Enhance visible light absorption and improve catalyst stability.	[91]
Pure water	Sono photocatalysis	50 W xenon lamp	(15)	Low yield, simple system without catalyst.	Extremely low efficiency, not suitable for large-scale applications.	Incorporate efficient catalysts to improve yield and scalability	[40]

absorbs on surface of the catalyst effectively. Under these circumstances, the catalyst surface may have enough OH groups to adsorb the molecules of the substrate.

Table 3 lists the stepwise mechanism for the photocatalytic H_2 evolution that was intended by Karimi Estahbanati et al. work. As a result, a photocatalyst's absorption of a photon initiates several reactions in the process. A photogenerated electron and hole are created because of this absorption reaction (a). The species produced by photolysis are incredibly reactive, and due to their high reactivity, photogenerated species frequently recombine quickly and produce heat reaction (b). However, the bulk ions of the substrate, water, and hydroxide create active sites on the surface (S) and start to adsorb. It can be seen by reactions (c)–(e). Reactions (f)–(h) indicate that the adsorbed particles can react with photogenerated holes, slowing down the reaction rate at species that are photogenerated recombine and suppressing process. The substrate either directly reacts shown in reaction (f) or indirectly shown in reaction (g) through the formation of hydroxyl radical's reaction (a) react with the photogenerated holes. The photogenerated electrons reduce the protons that were created from the substrate reaction (f) or water reaction (g) to create a hydrogen molecule reaction (j) [109]

Photocatalytic activity is more efficient in alkaline pH conditions than in neutral ones; in contrast, photocatalytic activity is slower in acidic regions than in neutral ones. The breakdown of methylene blue under UV radiation under different pH conditions was studied by Nasikhudin et al. using TiO_2 nanoparticles. It suggested that the UV light presence might start the performance of photocatalytic TiO_2 nanoparticles. The 15% breakdown of methylene blue (MB) does not do the photocatalytic activity; instead, the adsorption of (MB) blue by TiO_2 nanoparticles. Without UV radiation, photocatalytic activity is impossible. TiO_2 nanoparticles' photocatalytic activity is sensitive to pH. TiO_2 nanoparticles had 40% photocatalytic activity in acidic conditions pH = 4.1, (90%) in neutral conditions pH = 7.0, and (97%) in basic conditions pH = 9.7. The maximum photocatalytic activity takes place under base conditions when OH^- can react directly with a hole to form hydroxyl radicals (OH*) [110].

In Pelayo et al., study utilization of CdS as a photocatalyst with sacrificial agent Na_2S/Na_2SO_3, gives a higher H_2 production rate when using NSW compared to Artificial Seawater. Moreover, in NSW, carbonate/bicarbonate equilibrium acts as a buffer to keep pH near 10.0 ± 0.2 best out of H_2 production. As an illustration, Guan et al. [111] reported that, in comparison with pure water splitting, the HER was significantly upgraded by the incorporation of an aqueous NaCl solution. However, as seen in Fig. 6(a), the boosting

Table 3 Lists the stepwise mechanism for the photocatalytic H_2 evolution

Number	Stepwise Reaction Mechanism	Reaction pathways
(a)	Absorption of photon	$\mathrm{photocatalyst} + \mathrm{hv} \rightarrow \mathrm{e^-} + \mathrm{h^+}$
(b)	Recombination of photon	$\mathrm{e^-} + \mathrm{h^+} \rightarrow \mathrm{heat}$
(c)	Adsorption on active sites	$\mathrm{Sub} + \mathrm{S} \leftrightarrow \mathrm{Sub_{ads}}$
(d)	Adsorption on active sites	$\mathrm{H_2O} + \mathrm{S} \leftrightarrow \mathrm{H_2O_{ads}}$
(e)	Adsorption on active sites	$\mathrm{OH^-} + \mathrm{S} \leftrightarrow \mathrm{OH^-_{ads}}$
(f)	Direct transformation of substrate	$\mathrm{Sub_{ads}} + \mathrm{h^+} \rightarrow \mathrm{LP_{ads}} + \mathrm{h^+_{ads}}$
(g)	Trapping of holes	$\mathrm{H_2O_{ads}} + \mathrm{h^+} \rightarrow .\mathrm{OH_{ads}} + \mathrm{H^+_{ads}}$
(h)		$\mathrm{OH^-_{ads}} + \mathrm{h^+} \rightarrow .\mathrm{OH_{ads}}$
(i)	Indirect transformation of substrate	$\mathrm{Sub_{ads}} + .\mathrm{OH_{ads}} \rightarrow \mathrm{LP_{ads}} + \mathrm{H_2O_{ads}}$
(j)	Trapping of Electrons	$2\mathrm{H^+_{ads}} + 2\mathrm{e^-} \rightarrow \mathrm{H_2}$

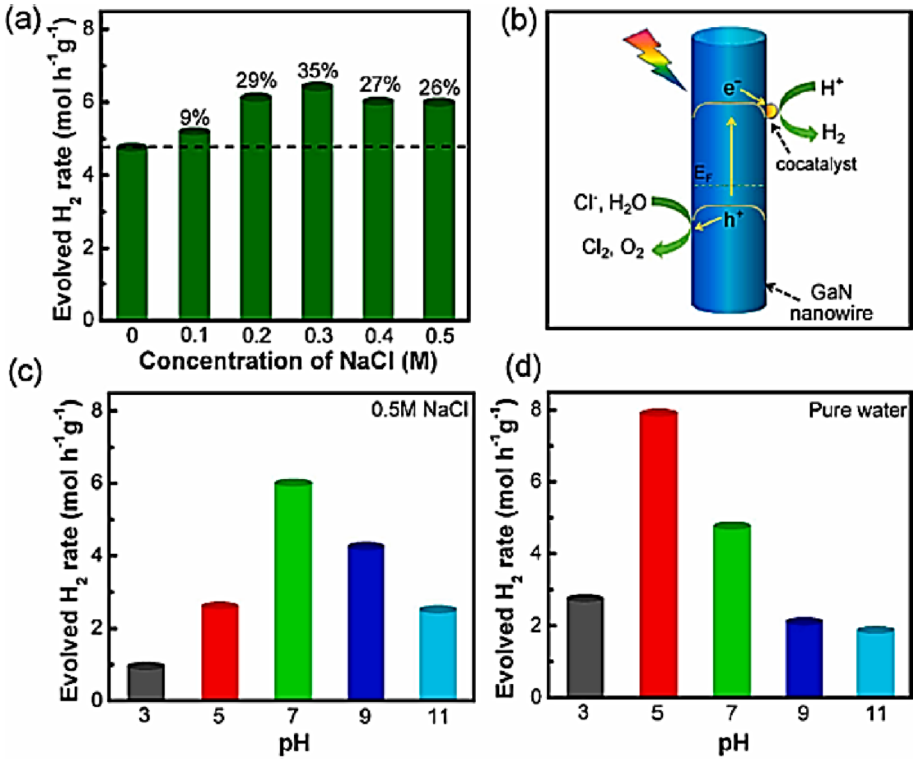

Fig. 6 (**a**) Photocatalytic H_2-evolution performance with modified p-GaN nanowire arrays, (**b**) Representation of the unsupported seawater splitting of a modified p-GaN nanowire, (**c**) HER in NaCl solutions with various pH values and (**d**) Water splitting under pure water [111]

tendency of the HER was reduced as NaCl concentrations increased above 0.3 M. Applying NaCl solutions in place of pure water significantly increased the generation of hydrogen. After the process, free chlorine which might be present as dissolved Cl_2, HClO, and/or ClO^- was measured and found to be about 0.1 mg/L, which was low in comparison to the evolved H_2/O_2 gases [86].

As a result, it was shown that although the Cl^- oxidation process did take place during the seawater splitting reaction, only a tiny amount of the products of the process were left in solution. Notably, the pH of the solutions was constant both before and after the reaction, and the ratio of evolving H_2 to O_2 was the optimal ~2:1 ratio. The process of seawater splitting may really use the chlorine oxidation reaction as an intermediary reaction. As shown in Fig. 6(b), below the photogenerated electrons in the p-GaN nanowire array's conduction band reduced protons to form H_2, whereas the photogenerated holes in the valence band could oxidize both H_2O and Cl^-. In fact, the following reaction could occur between dissolved Cl_2 and water:

$$H_2 + Cl_2 \rightarrow H^+ + Cl^- + HClO \tag{12}$$

and HClO could easily be decomposed under irradiation [112] according to the following reaction:

$$HClO \rightarrow 2H^+ + 2Cl^- + O_2 \tag{13}$$

Simulated seawater is used as 0.5 M NaCl, in addition to HCl or NaOH pH changes. Seawater splitting investigation using arrays of p-GaN nanowires shown in Fig. 6(c) at

various pH levels. At pH = 6.5, breakdown of $HClO/ClO^-$ took place under evolution of oxygen. According to electrolysis of industrial NaCl at neutral pH better performance is seen when NaCl solution as opposed to either acidic or basic solutions [113]. Figure 6(d) also illustrates the splitting of pure water at various pH values for comparison. At pH = 5, pure water splitting performed better compared to the ideal pH for GaN-ZnO photocatalysts. It is crucial to recognize that during the reaction, the solution's pH was constant. As shown in Fig. 6(c-d), The neutral conditions with a pH = 7.0 produced the best seawater-splitting results [111].

3.4 Effect of temperature

The catalyst's activity reduces at extremely low temperatures less than (0 °C), and the reaction rate is limited by desorption of final product on the catalyst surface. However, pollutants cannot be adsorbed at temperatures higher than 80 °C, which limits the photoreaction's potential [114, 115]. It is noticed that the photoreaction rate increases as the temperature rises in the 20–60 °C range [116–118]. When the procedure is conducted in natural sunlight, it is crucial to activate the TiO_2 surface and have a correct grasp of how the temperature affects the reaction rate. When employing a TiO_2 catalyst for photo disinfection, raising the temperature causes microorganisms to be inactivated more successfully [119].

Numerous investigations have demonstrated how temperature affects photocatalysis's efficiency [120–122]. In general, the temperature range for photocatalytic process should lie between (20–80 °C) [114, 121].

The Van't Hoff-Arrhenius equation describes the temperature dependence of the rate constant, with $\ln\left(\frac{k_1}{k_2}\right) = -\frac{E_a}{R}\left(\frac{1}{T_2} - \frac{1}{T_1}\right)$ where E_a is the activation energy, R is the universal gas constant, and k_1 and k_2 are the rate constants at temperatures T_1 and T_2.

By simply controlling the heating rate [93], developed four distinct tubular g-C_3N_4 morphologies that were produced using urea and melamine as basic precursor materials: stacked thin rectangular plates with flocculent structure, porous hollow tubes, porous hollow tubes, and tetragonal hollow prismatic tubes. Of these, the ragged porous hollow tubular g-C_3N_4 (TCN-1.5) maintains a high H_2 evolution rate (6782 μmol $h^{-1}g^{-1}$) from seawater. It exhibits an extraordinary hydrogen evolution rate of 8683 μmol h^{-1} g^{-1} from water, which is 19.3 times that of the massive g-C_3N_4 (449 μmol h^{-1} g^{-1}).

Mesoporous-assembled 0.93 TiO_2–0.07ZrO_2 mixed oxides are specific for H_2 production in relation to mesoporous-assembled pure TiO_2 and the impact of calcination temperature. The incorporation of this secondary ZrO_2 phase could not only effectively improve the mesoporous-assembled structure stability of the TiO_2 but also inhibits its anatase-to-rutile phase transformation during the calcination step up to 750 °C [70]. In a circulation system using a hot plate, the effects of the temperature shift brought on by solar heat were ascertained.

Under full-spectrum irradiation, Fig. 7 (a) demonstrates that the PC-HER rates of TiO_2 P25 rise with temperature from 25 to 65 °C. At 65 °C, it attains 152 μmol·$h^{-1}g^{-1}$, which is 6.1 times more than at 25 °C. According to a prior study by Kumaravel et al. (Kumaravel et al. 2019), several scavengers were compared for different photocatalysts. Ethylene glycol (EG) was chosen as the sacrificial agent since it was the most effective for TiO_2. Triethanolamine (TEOA) as a sacrificial agent for TiO_2 P25 and one weight% Pt–TiO_2 P25 in our investigation, but none of the catalysts showed any hydrogen evolution.

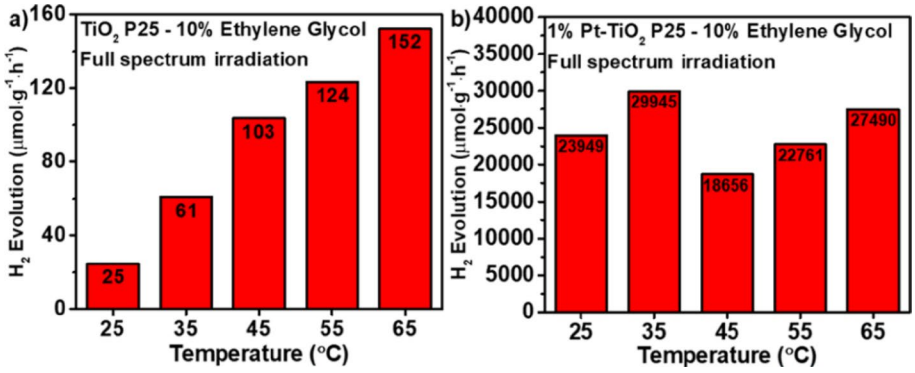

Fig. 7 H_2 evolution rate under different photocatalytic conditions: (**a**) TiO_2 P25 with 10% ethylene glycol, and (**b**) TiO_2 P25 loaded with 1 wt% Pt and 10% ethylene glycol. Reproduced from Zhang et al., "Enhanced hydrogen production via Pt/TiO_2 photocatalysts in ethylene glycol–water systems," ACS Sustainable Chemistry & Engineering, 2022, 10(15), 4853–4862, © 2022 American Chemical Society, with permission [123]

In another study by Bora et al., the photocatalytic H_2 evolution rate (PCHER) with 1 weight% Pt with TiO_2 P25 at 25 °C is 23,949 μmol·h^1g^{-1}, which is furthermore up to 958 times greater compared to the value of TiO_2 P25 at the same temperature, according to Fig. 7 (b). Interestingly, nevertheless, one weight% Pt in TiO_2P25 did not result in activity that increased steadily with temperature. At 35 °C, the photocatalytic H_2 evolution rate noticeably increases as 29,945 μmol·h^{-1} ·g^-, but at 45 °C, it decreases to 18,656 μmol·h^{-1} g^{-1}, then increases to 22,761 μmol·h^{-1} ·g^{-1} at 55 °C and 27,490 μmolh^{-1} g^{-1} at 65 °C. The highest value at 35 °C is still 8% higher than the value at 65 °C. Additionally, examined how sunlight heat affects at 25 °C, which is higher as well. At 25 °C, the (PCHER) rate of the catalyst one weight% Pt-g-C_3N_4 is 1684 μmolh^{-1} g^{-1} [123].

3.5 Effect of light source

When an electromagnetic (EM) wave an incident light ray runs into an obstruction or no homogeneity, in this case, the scattering particle, light is redirected. This phenomenon is known as scattering of light. An electron's orbits within the discrete particle's constituent molecules are regularly disturbed by the electromagnetic wave's interaction with it at a frequency (o) equal to the incident wave's electric field [124]. The light scattering by an induced dipole moment due to an incident EM wave. An induced dipole phenomenon is a continuous separation of the charges, created by the electron cloud's oscillation or turbulence inside the molecule. The oscillatory-induced dipole moment, which appears as an EM radiation source, scatters light. The process by which most of the light dispersed from an element release at exactly the equal frequency (o) as the incident light this process is known as elastic scattering. Light scattering is a complex interaction between incoming electromagnetic radiation and the molecular/atomic configuration of the scattering object, rather than merely the electromagnetic waves or incident photons "jumping" off the exterior layer of an encountered object [125].

Until Albert Einstein brought it back to life at the close of the 19th century, the idea that light is a particle had virtually disappeared. Since light's dual nature as "both a wave and a particle" was previously established, quantum mechanics has replaced electromagnetics as the fundamental theory [126]. According to Einstein, light is a kind of particle called a photon, and photon movement is a wave [127]. The fundamental idea of Albert Einstein's light quantum concept is that the energy of light is proportional to the

frequency of its oscillations. According to his theory, the energy of photons is equal to "Planck's constants times oscillation frequency," where the photon energy is the oscillation frequency's height, and the light's intensity is the number of photons [128]. The behavior of tiny particles known as photons, which are imperceptible to the human eye, carries responsibility for the diverse characteristics of light, a form of electromagnetic wave [129]. The color of some compounds clearly distinguishes them from one another. Thus, 2,4-dinitrophenylhydrazone derivatives of aldehydes and ketones, quinone is yellow, aspirin is colorless, chlorophyll is green, depending on double bond conjugation, range in hue from bright yellow to deep red.

In this way, the human eye analyzes light that is reflected from solid surfaces or flowing through liquids, acting as a spectrometer. Sunlight, often known as white light, is made up of a wide variety of radiation wavelengths in the ultraviolet (UV), visible, and infrared (IR) regions of the spectrum, even though we perceive it to be uniform or homogenous in color. Sunlight can be passed through a prism to divide the visible portion's component colors, as seen on the right. By sending sunlight through a prism that operates to bend the light in varying degrees according to wavelength, the visible portion's component colors [66].

Photocatalysis takes advantage of how energy, wavelength, and frequency interact across the electromagnetic spectrum. In simple terms, it uses light whether ultraviolet (UV), visible (VIS), or infrared (IR) to excite a photocatalyst and initiate chemical reactions. UV light, with its high energy and short wavelengths, is particularly good at activating materials like titanium dioxide (TiO_2), producing energetic charge carriers that can break down pollutants or split water into hydrogen and oxygen. Visible light, which carries less energy, has become increasingly important thanks to new photocatalysts designed to work effectively with sunlight. Infrared light, though lower in energy, plays a supporting role by adding heat to boost certain processes. This fascinating interplay between the properties of several types of light is helping to drive forward sustainable technologies and innovative chemical solutions. Among the light sources utilized in photocatalysis are Visible, UV and IR. More details on each type are described below (Kuipers 2014).

Visible light and other electromagnetic radiation are frequently seen as wave phenomena with a particular wavelength or frequency. The wavelength, which can be expressed in meters, centimeters, or nanometers (10–9 m), is defined as the separation between neighboring peaks (or troughs) on the left below. Frequency is the total quantity of wave cycles that pass a specific area in each amount of time. It is often stated in revolutions per second or hertz (Hz). The range of visible wavelengths is roughly 380–760 nm. Red has the longest wavelength that can be seen, whereas violet has the shortest. The wavelengths of the visible region of the spectrum correspond to the colors that humans experience. Wavelength increases as one move from left to right in horizontal diagrams, like the one shown on the bottom left. The energy required to drive electrons from the semiconductor's valence band to its conduction band and start the reaction that splits water molecules into hydrogen and oxygen is provided by visible light in these processes.

UV lights are divided into three categories: UV LED (A, B, C) and UVA LED, which are commonly employed to remove organic pollutants in lab-grade water. UVB and UVC LEDs are utilized in UV/H_2O_2 and Photo-Fenton-like pollution remedies. UV radiation is sufficiently intense to encourage electrons to move from lower-energy orbitals to

higher-energy ones, which could cause bond breakup [130]. The absorption band edge of the photocatalyst material determines the range of light sources that can be used in photocatalysis [131].

UV-enhanced light sources, such as xenon arc lamps, are employed for materials like TiO_2 and ZnO that have absorption band edges between 300 and 400 nm. UV-enhanced spectrum light sources, such as xenon arc lamps with filters or high-power LED light sources, are employed for materials with absorption band edges between 400 and 800 nm, such as CdS, g-C_3N_4, and $BiVO_4$.The crucial information about molecular structure from UV-Vis spectroscopy, such as the number of pi bonds in a molecule, the presence of carbonyls (C = O), whether or not pi links are conjugated, and more. Photons with wavelengths between 2500 and 25,000 nm promote vibrating energy levels in bonds. A longer wavelength also indicates that these photons have fewer electrons compared to photons of visible light because E = hv and c = νλ.

As shown in Fig. 8 (a) below, TiO_2 has the lowest possible H_2 performance of 2.21 mmol/g/h, because of a high rate of recombination of electrons and holes in pure water. Under visible light, however, TiO_2-rGO's H_2 generation rate is 4.41 mmol/g/h, which is more than twice as high as TiO_2. Simultaneously, TiO_2-Cu generated H_2 at a rate of 14.17 mmol/g/h, which was roughly seven times higher than TiO_2. The H_2 generation rate of TiO_2-rGOCu can reach 18.13 mmol/g/h, which is approximately 8.2 and 4 times higher than that of TiO_2 and TiO_2-rGO., accordingly. The best water-splitting photocatalysts should be highly stable and have outstanding catalytic activity. Stability studies on TiO_2-rGO-Cu were conducted to assess this property. Following six photocatalytic cycles Fig. 8 (b), this material's H_2 generation activity in seawater simulation drops by 35.5% [90].

In another study, Xiong et al. [91] developed Well-defined Z-scheme $Na_2Ti_3O_7$/Ag/CdS ($N_{10}A_1C_5$) multidimensional heterojunctions were created by assembling two-dimensional CdS nanoplates, one-dimensional $Na_2Ti_3O_7$ (NTO) nanotubes and zero-dimensional Ag nanoclusters. Zero-dimensional Ag nanoclusters applied to the surface of NTO nanotubes not only act as an electron mediator in the creation of the Z-scheme between NTO and CdS, also supply hot electrons through their plasma effect. Together, Ag nanoclusters and CdS nanoplates function as visible light absorbers, enhancing the absorption range and intensity of visible light. The resulting Z-scheme N_{10} A_1C_5 heterojunctions under visible light source shows an H_2 generation of 1793μmol/(g·h) in sea water splitting photocatalyst An easy one-pot microwave-assisted synthesis produced by

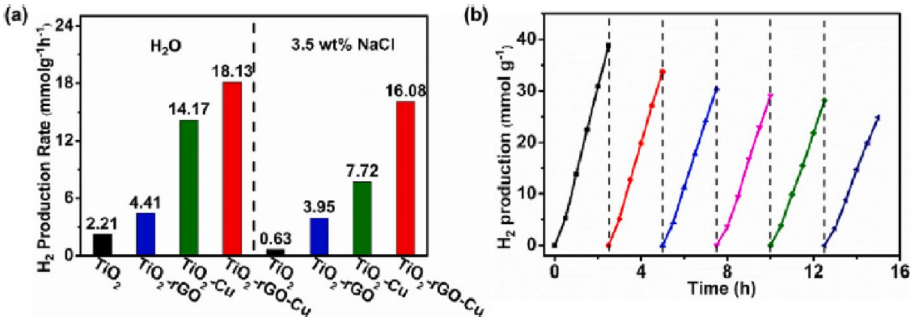

Fig. 8 Rate of photocatalytic H_2 synthesis in water and seawater simulation (b) stability of TiO_2–rGO–Cu in the presence of light (250–780 nm). Reproduced from Lei Xia, Yi Lu, Yuan-Zhou Li, et al., "TiO_2-rGO-Cu complex: A photocatalyst possessing an interfacial electron transport mechanism to enhance hydrogen production from seawater," Chemical Physics Letters, 822, 140,498 (2023). © 2023 Elsevier. Reprinted with permission from Elsevier [90]

Lin et al. [88], a novel heterostructure of In_2S_3/In_2O_3 nanosheets free of noble metals for photocatalytic water splitting triggered by blue LED light.

Under blue-LED light irradiation, In_2S_3/In_2O_3 nanosheets can grow with increased photocatalytic water splitting for hydrogen production if the proper $InCl_3$ concentrations and reaction temperatures are used. Furthermore, under blue-LED light irradiation, the improved In_2S_3/In_2O_3 nanosheets showed a greater hydrogen generation rate of 618.0 $\mu molh^{-1}g^{-1}$ in seawater without modified pH values. Moreover, the four cycles of increasing photocatalytic hydrogen production efficiency were demonstrated by the reusable In_2S_3/In_2O_3 nanosheets. The reason behind this phenomenon is the reaction between In_2S_3/In_2O_3 nanosheets and seawater, resulting in the formation of $In_2S_3/In_2O_3/In(OH)_3$ nanosheets. These nanosheets can enhance the recombination of photogenerated charge carriers and their ability to harvest light, hence promoting their photocatalytic H_2 production.

H.Van et al., (2022) under simulated sunlight illumination, a novel heterogeneous Pt/GaP-C3N4 (PGC) photocatalyst was developed and used for natural seawater and artificial seawater. An introduction of PGC photocatalyst, the hybrid heterojunction structure of GaP-C_3N_4 suppresses the recombination rate of photogenerated electron-hole pairs and encourages a Z-schematic electron migration. An innovative composite photocatalyst comprising g- C_3N_4 and GaP with loaded Pt (Pt/GaP-C_3N_4) was created by combining ionothermal, thermal, and photo-deposition methods to improve sunlight-driven seawater splitting. Measurements were made of the evolution rates of hydrogen and oxygen (HER/OER) in various water sources. The rates in deionized water were 23.4 μmol g^{-1} and 46.5 μmol g^{-1}, respectively. For artificial seawater, they rose to 34.3 and 65.5 μmol h^{-1} g^{-1}. The rates for natural seawater splitting were 53.9 and 24.9 μmol $h^{-1}g^{-1}$, respectively [92].

The representation of the mid-infrared (IR) portion of the spectrum raises the possibility that we might be able to learn more about the makeup of a molecule's bonds if we measure the area where it absorbs infrared light [132]. According to Fiorenza et al. [133] pulsed laser irradiation was applied to water-soluble TiO_2 suspensions (first approach), and it caused structural changes on the surface and in the bulk of the material. The increased amount of H_2 produced under UV light irradiation is 20,900 $\mu mol{\cdot}g^{-1}{\cdot}h^{-1}$. the second technique was based on a synthesizing method to generate TiO_2 with a macroporous structure to promote an effective absorption of sunlight process inside the material pores and enable a high H_2 generation of 640$\mu mol{\cdot}g^{-1}{\cdot}h^{-1}$according to solar light irradiation [134].

Transforming sunlight into a portable and stable energy source has been a major area of research. Among the various systems studied, semiconductor-based photocatalysts for hydrogen production have gained significant attention. Commercially available TiO_2 stands out for its affordability, chemical stability, non-toxicity, and excellent photostability [135]. However, it does have two notable limitations: its wide band gap (3.0 – 3.2 eV), which confines its light absorption to the ultraviolet range and excludes the visible spectrum [136]. In Fig. 9, the photocatalytic process of TiO_2 is described below.

An electron will migrate from the band known as the valence band to the conduction band when the energy of the light shining on a TiO_2 semiconductor is higher than the band gap, creating holes (h^+_{vb}) in the valence band and electrons (e^-_{CB})in the band of conduction. Superoxide radicals (O_2^{-*}) are created when electrons encounter the

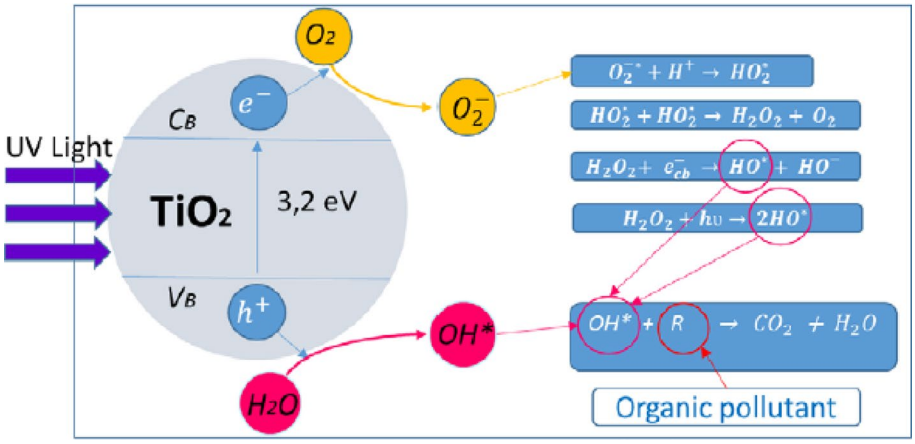

Fig. 9 TiO_2 Photocatalytic Mechanism [110]

surrounding oxygen and hydroxyl radicals (HO^*) are created when holes react with the surrounding water.Both free radicals will meet nearby water-soluble substances, particularly organic substances or polymers. This hydroxyl radical will break down the organic molecule or polymer into Both carbon dioxide (CO_2) and water (H_2O). Superoxide radicals ((O_2^{-*})) will react with water (H_2O). to form hydrogen peroxide (H_2O_2), which will then react with electrons to form hydroxyl radicals. Peroxide (H_2O_2), will also react with light energy (hü) to form a hydroxyl radical (HO^*). This hydroxyl radical will break down the organic polymer (R) (HO^*) into carbon dioxide (CO_2) and water (H_2O) [110]. Improved charge separation rate, possibly as a result of superior absorption capabilities for visible light [133].

To evaluate the charge transfer and recombination rates, as well as the movement of charge carriers in TiO_2, TiO_2-rGO, TiO_2-Cu, and TiO_2-rGO-Cu, we conducted electrochemical impedance spectroscopy (EIS) tests. Without light, the electrochemical impedance follows this order: TiO_2 > TiO_2-rGO > TiO_2-rGO-Cu > TiO_2-Cu. Under light, the order of the curve radius changes to: TiO_2 > TiO_2-Cu > TiO_2-rGO > TiO2-rGO-Cu. The EIS curves show arc shapes due to charge migration, and a smaller arc radius indicates better separation of photogenerated electrons and holes [137]. The smaller arc radius of TiO_2-rGO-Cu indicates it does a better job of separating electron-hole pairs. This was further confirmed through photoluminescence (PL) spectroscopy, which showed that TiO_2-rGO-Cu has excellent carrier separation efficiency. The high electron mobility of rGO and the electron-accepting role of Cu nanoparticles help reduce the recombination of photogenerated electron-hole pairs. As a result, the intensity of PL peaks between 400 and 500 nm, generated by 315 nm laser excitation, decreases in this order: TiO_2 > TiO_2-rGO > TiO_2-rGO-Cu [138].

Another study by Díaz et al. [139] shows low-cost M/TiO_2 semiconductor catalytic reactions were made by impregnating a commercial titania substrate with five distinct rows of transition-metal elements (M = Fe, Co, Ni, Cu, or Zn) to enhance the photocatalytic performance of titanium dioxide to UV and visible light for the hydrogen production. The Cu/TiO_2 photocatalyst demonstrated the highest efficiency in hydrogen synthesis, with production rates of approximately 5000 and 220 μmol h^{-1} g^{-1} H_2 for ultraviolet and visible irradiation, correspondingly. When exposed to UV light, Ni/TiO_2 and Co/TiO_2 also demonstrated a notable photocatalytic activity [140].

For instance, a highly effective directional interfacial electron transport mechanism is suggested by Xia et al. [93] in his work TiO_2_rGO-Cu photocatalyst is engineered to have a directed electron transfer channel from nitrogen-doped TiO_2 to rGO and subsequently to Cu nanoparticles, resulting in effective separation of electron-hole pairs. A xenon light source (type PLS-SXE-300UV, wavelength range (250–780 nm) is then used to evacuate and irradiate the entire system. To determine the H_2 concentrations, the produced gas was gathered and subjected to gas chromatography using a TCD detector. The findings indicate that in artificial seawater, TiO_2_rGO-Cu has a hydrogen production rate of 16.08 mmol h^{-1} g^{-1}, up to 25 times greater than that of TiO_2 [90]. A little portion of the spectrum of electromagnetic waves is made up of infrared and ultraviolet radiation. The wavelength of IR ranges is divided into three categories states as: -shortwave infrared radiation (SWIR), which ranges from 780 to 1500 nm; medium-wave IR (MIR), which ranges from 1.5 to 4000 nm; and long-wavy IR (FIR), which ranges from 4000 nm to 1 mm, are the three categories of infrared radiation. The infrared spectrum is a region having a longer wavelength.

The sun is the primary source of infrared radiation on Earth. A UV spectrum is the region next to visible light that has a shorter wavelength. Each wavelength transports a specific quantity of energy. The shortest the wavelength and more tremendous the energy the radiation can carry, the faster the frequency of such waves. Therefore, more energy is transferred into radiation at higher frequencies, and shorter wavelengths imply that short-wavelength radiation can reach deeper into materials. In theory, (IR) is not dangerous to humans because its wavelength is greater than that of visible light. Naturally, you must always consider that the product and nearby components may also get heated by the application or heating of the substance. In the Gannoruwa et al. study [141], they examined an IR photonic active catalytic system that converts solar energy to chemical energy.

They present an efficient "Dark Photocatalyst" for water photolysis. Using a straightforward chemical deposition technique, the Ag_2O/TiO_2 composite catalyst which has 28% silver and 72% titanium was created. Low-energy 800–1200 nm IR radiation was used to demonstrate hydrogen production for the first time, and it was discovered that the catalyst was active in the dark or in the infrared portion of the solar spectrum. The essential results are shown in Fig. 10 from [142]. A (1% wt.) Cu_2O/TiO_2 combination photocatalyst made by ball milling (200 rpm, 1 min) at an environment temperature of 80 °C and a high-pressure mercury lamp yield maximum AQE measurements of 3.17% and 6.54% under the age of visible-light radiation in a solution of methanol as and glycerol, respectively. The highest light-to-chemical energy efficiency values for methanol and glycerol under the same conditions are 1.16% and 2.36%, respectively.

Furthermore, the efficiency values achieved in the range of visible light (AQE = 1.56%, $\eta = 0.56$) are only marginally lower than those obtained employing UVA + visible light radiation under the same conditions (T = 35 °C, methanol as a scavenger) (AQE = 2.31%, $\eta = 0.83$). As shown in Fig. 10 above, the various light intensities really cause similar effects in terms of the quantum yield and light-to-chemical energy efficiency, even though there is a significant difference in hydrogen creation between either the presence or the absence of UVA radiation [142]. Over 50% of the sunlight that reaches the earth is infrared (760–5300 nm), 42% is visible (400–760 nm), and 5% is ultraviolet (UV 290–400 nm) [139].

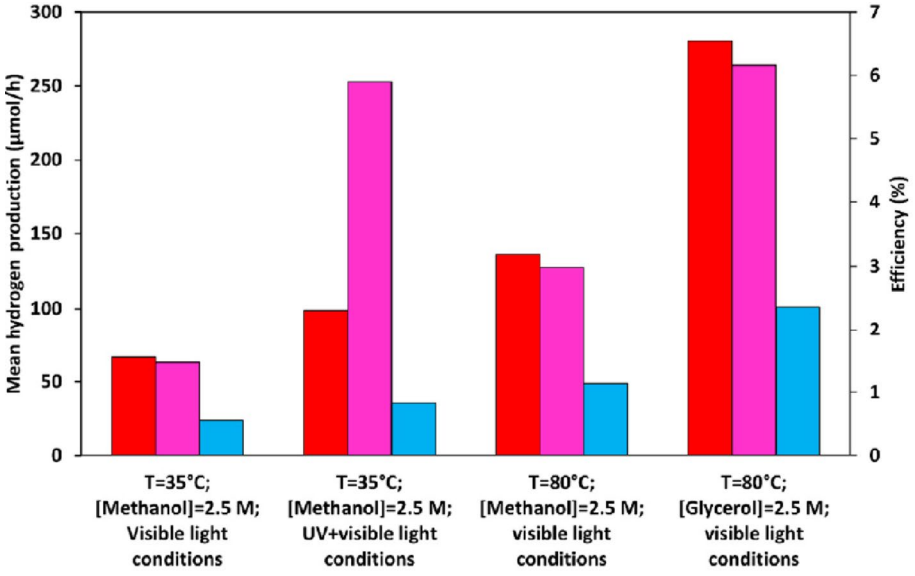

Fig. 10 Mean hydrogen evolution rate (■), AQE (■), and η (■) obtained under visible light radiation (λ > 400 nm) and UV-A + Visible light conditions [142]

The most sustainable and cleanest source of energy for our everyday needs is solar energy. A semiconductor's photocatalytic hydrogen evolution process (PCHER) is one of the most promising methods for converting sunlight into chemical energy using hydrogen molecules. Due to the ability to absorb infrared light in the solar spectrum, the reaction temperature in (PCHER) processes can be significantly increased without temperature control [143, 144]. When it comes to producing hydrogen (H_2), UV light is generally thought to be more efficient than visible and infrared (IR) light because of its higher energy, which enables more effective excitation of the electrons in photocatalysts and improves H_2 generation. Since several photocatalysts, including titanium dioxide (TiO_2), efficiently absorb UV light, UV light is frequently used in photocatalysis [145]. The photocatalyst's electrons can be excited by the tremendous energy of UV photons, creating electron-hole pairs that fuel the water-splitting cycle and produce hydrogen. Nevertheless, UV light becomes less prevalent in natural sunshine and could need more energy, which makes it less practical for large-scale uses [146].

Recent developments in the production of hydrogen via photocatalytic processes have made visible light extremely important since certain photocatalysts have been designed for absorbing visible light [146]. The absorption of visible light can be improved by doping TiO_2 with components such as nitrogen or by forming composites with carbon-based materials. In terms of efficiency, natural sunlight contains more visible light (about 43% of the solar spectrum), which makes it a more efficient and sustainable energy source for real-world uses. However, photocatalysts' capacity to absorb light and produce charge carriers is a significant factor in how effective they are in visible light [145].

In contrast, IR light has a lesser amount of energy and predominantly induces molecular vibrations rather than electronic transitions, which are essential for the photocatalytic process. Since visible and UV light has higher energy than infrared light, electrons found in conventional photocatalysts like TiO_2, which require more energy to cross their bandgap, are usually not excited by infrared light [147].To restrict the direct contribution of infrared light to photocatalytic processes. Even though sunlight contains a lot

of infrared light (about 49% of the solar spectrum), this energy mainly heats the photocatalyst and the liquid surrounding it instead of immediately assisting in the excitation of electrons to produce hydrogen in terms of efficiency. Some sophisticated photocatalytic systems (such as photothermal systems) are made to increase reaction rates by using the heat produced by infrared light. However, recent research is looking into ways to use IR light with materials that can absorb and transform its energy into forms that can be used to produce H_2 [134]. The comparison of three light sources is illustrated below in Fig. 11.

The main concerns discovered are inadequate distinguishing between photogenerated limited surface area, and a narrow absorption range in the electromagnetic spectrum. These challenges come because of the current catalyst's improper band edge potential and a large bandgap [148]. Furthermore, to enhance water-splitting efficiency, photocatalysts have been modified with co-catalysts or dopants using various techniques. These include Z-scheme systems, hybridization processes, tuning crystallinity and morphology, adjusting band edge positions, narrowing the band gap, and optimizing surface structures. These modifications allow photocatalysts to absorb more light across the UV, visible, and infrared (UV-VIS-IR) regions [148].

3.6 Effect of dissolved oxygen

Hydrogen (H_2) and oxygen (O_2) can dissolve in water, photocatalytic overall water splitting (OWS) takes place under aerobic conditions. Compared to the most advanced OWS activity, the dissolved amounts of H_2 and O_2 are significant, as reflected by their Henry's law constants in water is 0.78 mmol L^{-1} atm^{-1} for H_2 and 1.3 mmol l^{-1} atm^{-1} for O_2 at 25 °C. However, H_2 dissolves less easily in water than O_2. As a result, in a photocatalytic (OWS) system where oxygen is initially removed, H_2 evolution rate to the O_2 evolution ratio should exceed as 2:1 during the early stages. The oxygen evolution process includes the formation, growth, and release of O_2 bubbles Fig. 12 (b) as well as the dissolution of oxygen into water Fig. 12(a). Initially, the oxygen evolution reaction (OER) generates molecular oxygen on the surface of the photocatalyst. Because the system starts out free

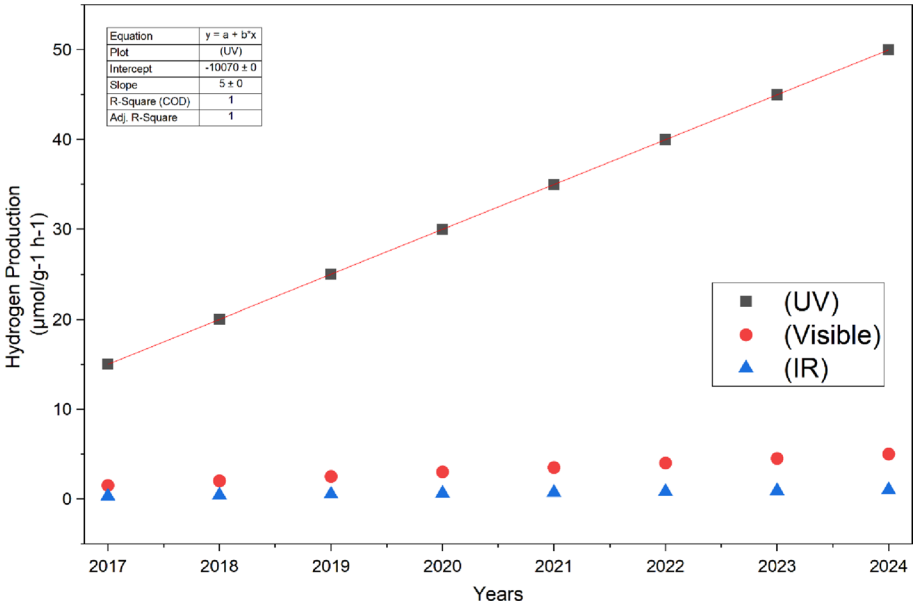

Fig. 11 Comparison of UV, VISIBLE and IR

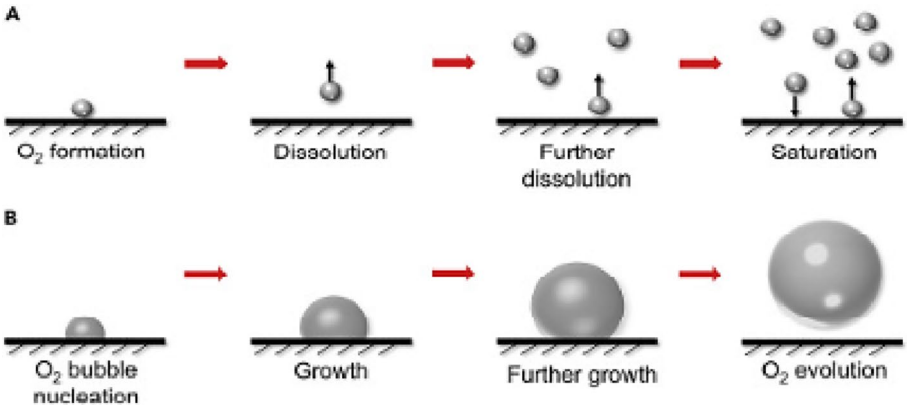

Fig. 12 (**a**) The breakdown of produced oxygen in water; (**b**) O_2 bubble evolution

of O_2, the concentration gradient and hydrogen bonding between O_2 and H_2O drive the freshly produced oxygen to dissolve into the surrounding water. As more oxygen is created, the amount of dissolved oxygen in the water gradually increases. A dynamic dissolution equilibrium is reached when the water's dissolved oxygen content achieves saturation. The O_2 that is subsequently produced may attach to the photocatalyst's surface. The unstable molecular O_2 tends to cluster and nucleate because of its high surface energy.

First, the oxygen nuclei attach firmly to the photocatalyst surface and progressively expand into small bubbles. Moreover, large bubbles absorb tiny bubbles because of Ostwald ripening. Due to decreased surface energy, oxygen bubbles are kept spherical throughout growth. As a result, the adhesion force is weakened as bubbles develop on the surface of photocatalyst because their contact area decreases. The bubbles separate from the surface and float to the top when they get large enough because the buoyancy force outweighs the adhesion force. In conclusion, water must reach its oxygen saturation point before oxygen bubbles appear and they get big enough (hydrogen evolution goes through a similar process) [149]. Additionally, oxygen hinders the process of producing H_2. With ease, oxygen joins electrons to create superoxide radicals (O_2·–), which are then transformed into water or H_2O_2. Figure 13 shows the oxygen reduction reaction competitive to HER [112]. Photocatalytic H_2 generation is negatively impacted by this undesired competitive reaction [149].

3.7 Effect of catalyst loading

Among the most important variables affecting photocatalytic effectiveness and cost management is catalyst loading [150]. Increasing the dosage produces more e^-/h^+ couples in addition to additional active sites for the pollutant's adsorption. As a result, photocatalysis rises as catalyst loading does. However, excessive dosage frequently causes the catalyst to aggregate, making the effluent murky and preventing the irradiation light from penetrating the effluent's internal mass. Lack of light inhibits the photogeneration of the electron hole pair and consequently photocatalysis. Therefore, to prevent overuse and guarantee optimum photonic efficiency, an ideal catalyst loading value must be utilized [123].

The impact of the loading of the catalyst on degrading performance has been documented because more significant amounts of e^- and h^+ can produce more active radicals,

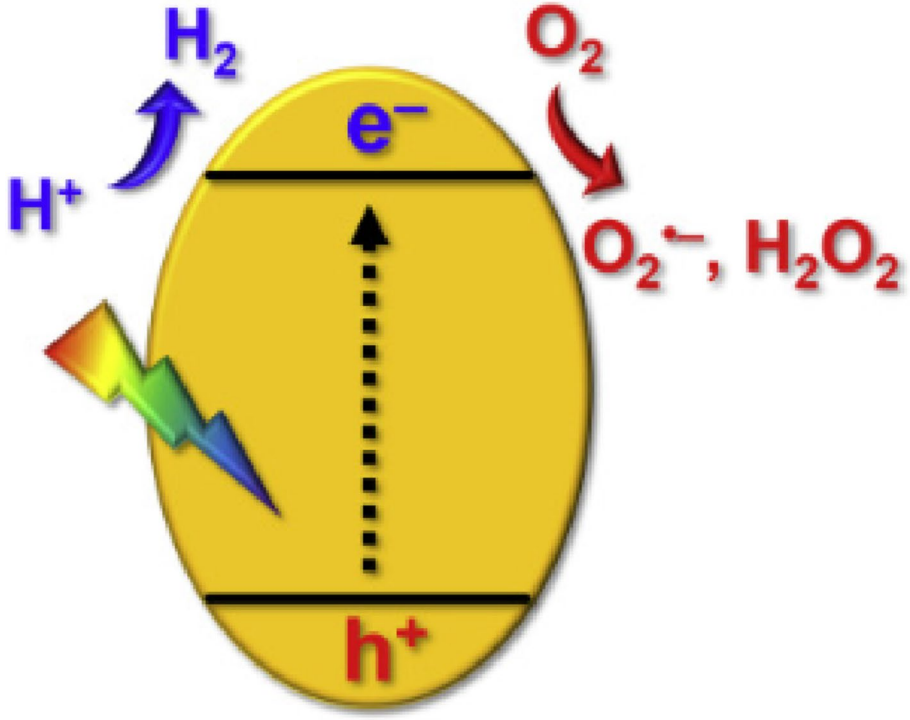

Fig. 13 Oxygen reduction reaction (ORR) competitive to HER [149]

and photocatalyst loading is more significant at an appropriate interval. Therefore, the amount of photocatalyst was proportionate to the photocatalytic performance [151]. According to earlier studies, the rate increased in direct proportion to catalyst loading but began to fall at extremely high levels when light scattering and screening effects tended to decrease. Agglomeration (particle-particle contact) causes the photocatalyst's surface area to decrease at high catalyst loading, which may have an impact on light absorption [152].

The amount of active surface available for degradation processes and adsorption increases as the catalyst loading increases. However, when the turbidity of a solution rises, photon penetration into the stream is constrained [153]. Additionally, water can be treated and disinfected via surface photocatalysis. As TiO_2 particles aggregate at large solid concentrations, a 497 reduction is also discernible. As a result, the catalyst mass directly correlates with the photoreaction's initial rate and efficiency [154]., However, the rate of reaction is unaffected by critical dose once it is reached and stays constant or even falls as the catalyst loading rises. Figure 14 (a) indicates a decrease in the aqueous rhodamine 6G (R6G) dyes' absorption peak intensity at 518 nm with respect to irradiation time. Plotting C/C_o against irradiation time in Fig. 14 (b) reveals that the curves exhibit a sharp decline for the first twenty minutes, after which the degradation slows down throughout the entire duration. CuO and CdS clearly show a slower rate of degradation compared to CdS/CuO, and this rate rises with the composite's CuO concentration increases. According to the pseudo-first-order kinetic model, which is represented by the formula $\ln (C_t/C_o) = -k_t$, where C_o is the initial dye concentration, C_t is the residue concentration at any given time, t, and k is the first-order kinetic rate constant, photodegradation of aqueous dyes should occur.

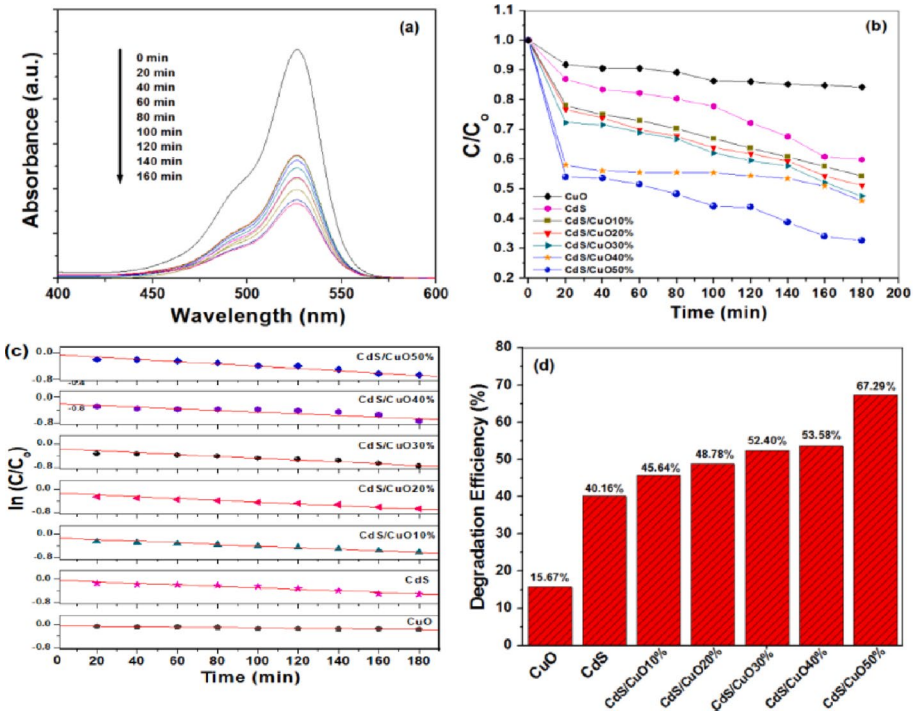

Fig. 14 Changes in the absorption spectra over time with irradiation are shown in (**a**) (**b**) illustrates the relationship between C/C_0 and irradiation time (**c**) shows $\ln(C/C_0)$ plotted against irradiation time and (**d**) presents degradation efficiency over the same period. Reprinted from Journal of Environmental Chemical Engineering, 347, 134,589, Nor Azlia Binti Aziz and Chan Kok Sheng, "Changes in absorption spectra and photocatalytic degradation kinetics under irradiation," © 2023, with permission from Elsevier [157]

As shown in Fig. 14 (c), the slope change in the line fitted to the ln(C/Co) graph helps confirm the rate constant. The regression constants (R^2) and rate constants (k) are as follows: 0.000781 min^{-1} (0.912) for CuO, 0.00260 min^{-1} (0.976) for CdS, 0.00277 min^{-1} (0.956) for CdS, 0.00302 min^{-1} (0.956) for CdS/CuO10%, 0.00320 min^{-1} (0.944) for CdS/CuO20%, 0.00246 min^{-1} (0.726) for CdS/CuO30%, and 0.00469 min^{-1} (0.901) for CdS/CuO50%. Among these, CuO shows the poorest photocatalytic performance, with the lowest degradation rate and efficiency. This is likely due to the rapid recombination of charge carriers generated by photons within its narrow band gap [155, 156].

When CuO is loaded into the composite, the rate increases constantly. Because of its most considerable rate constant, CdS/CuO50% is deemed the most effective photocatalyst among them. Furthermore, compared to CdS and CuO alone, CdS/CuO exhibits a superior photocatalytic degradation effect. When compared with CuO and CdS, respectively, the rate constant of R6G dye degradation when using the CdS/CuO50% catalyst increases by roughly 51% and 80%. However, Fig. 14 (d) shows the degrading rates of CuO, CdS, and CdS/CuO on R6G dye. When compared to CuO and CdS, the CdS/CuO photocatalysts exhibit greater degrading efficiencies. As the CuO catalyst content rises from 0 weight% to 50 weight%, which is 329% and 68% greater than that of CuO and CdS, respectively, the efficiency of degradation of CdS has been effectively increased from 40.16% to 67.29%, despite CuO having the smallest degradation percentage of only 15.67%. This finding implies that there has been a more significant synergistic impact between these two chemicals, which enhances their photocatalytic degradation capabilities [157].

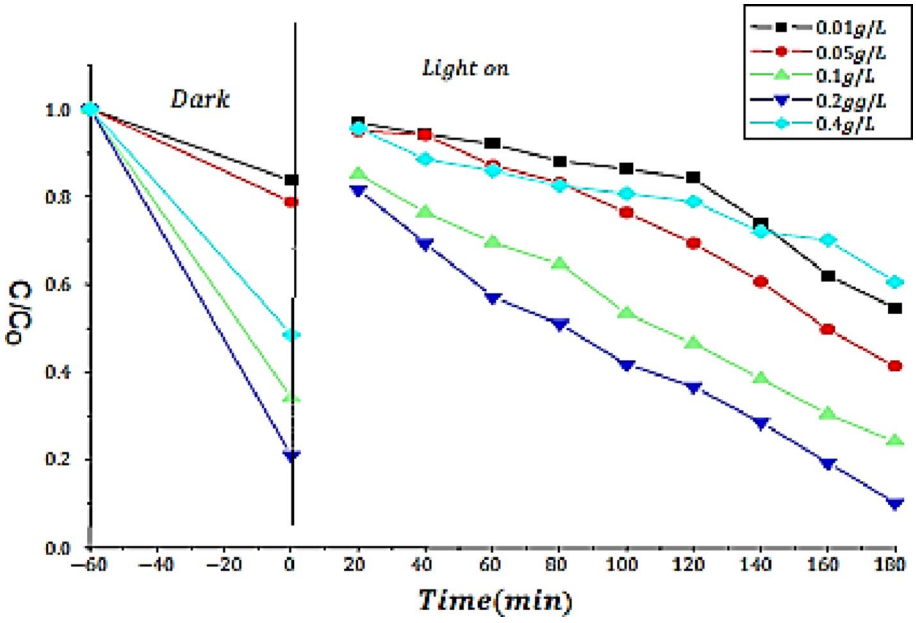

Fig. 15 Effect of catalyst loading vs. Irradiation time [86]

Amorphous FexP can be used to construct a bifunctional nanosheets-assembled CoMoP-FexP/NF that is superhydrophilic and has good electrocatalytic performance for the oxygen evolution reaction (OER) and hydrogen evolution reaction (HER). Using a moderate solvothermal technique, a novel amorphous FexP was successfully synthesized and bonded to the exterior of $Mn_{0.3}Cd_{0.7}S$ nanorods in this study. Compared to $Mn_{0.3}Cd_{0.7}S$ alone, the FexP/$Mn_{0.3}Cd_{0.7}S_{-0.2}$ combination generated 31.42 μmol g^{-1} h^{-1}, which is 766.34 times higher. Amorphous FexP was used as a great cocatalyst and electron collector to reduce carrier recombination, speed up e-transfer, and provide reaction sites for H_2 evolution and considerably enhancing the catalytic efficiency and stability of FexP/$Mn_{0.3}Cd_{0.7}S$ [58].

To evaluate the catalyst stability, Pelayo et al. (2024) demonstrated five cycles for five hours each using CdS as the catalyst was conducted as shown in Fig. 15 below. To eliminate any leftover air and the hydrogen created during the experiment, argon was used to purge the reaction media after each run. It takes a few hours for the photocatalyst to activate before it can produce as much hydrogen. After that, the rate of photocatalytic production remains constant. Additionally, the findings of an experiment showed the rate of H_2 evolution was 3.9×10^2 μmol.h^{-1}.g^{-1} until 70 h, after which it dropped to 2.7×10^2 μmol.h^{-1}.g^{-1} [86].Adjusting the catalyst loading between 0.01 and 0.4 g per liter shows the effect of a photocatalyst loading on the breakdown of organic pollutants. According to this study, methyl orange (MO) degradation first rises when the photocatalyst load increases between 0.01 g per liter and 0.2 g per liter. Nevertheless, the degradation of (MO) is reduced when the catalyst loading is increased from 0.2 g per liter to 0.4 g per liter, which might be because of an uneven distribution of light intensity that seems to be the result of overloading.

Consequently, a higher dosage of photocatalyst would result in a decreased reaction rate. The breakdown of the organic molecule (MO) should also be lower for lower photocatalyst loading, suggesting more light is passed through reactor and less radiation is transfer this might be because of an uneven distribution of light intensity that seems

to be the result of overloading. Consequently, a higher dosage of photocatalyst would result in a decreased reaction rate. The degradation of the organic molecules should also be reduced at lesser photocatalyst loading, which suggests that more light is passing through the reactor and that less of that light is being used for anything other than the photocatalytic activity [158].

Figure 15 below shows the effect of catalyst loading (0.01–0.4 g/L) vs. irradiation time on pollutant degradation under dark and illuminated conditions. In the dark stage, higher catalyst loadings lead to stronger adsorption, but the real photocatalytic activity is revealed after light irradiation. Among the tested dosages, 0.2 g/L achieves the most efficient photocatalytic performance, as seen by its steep decline in C/C0C/C_0C/C0 with time, indicating the highest rate of degradation. At lower dosages (0.01–0.1 g/L), the limited number of active sites restricts photocatalytic activity, while at the highest dosage (0.4 g/L), the performance decreases due to excessive turbidity and light scattering, which reduce photon penetration and catalyst activation. Therefore, an optimal dosage exists (here ~ 0.2 g/L), where sufficient active sites are available without significant light-shielding effects, making it the most suitable condition for maximizing both photocatalysis and hydrogen production efficiency.

4 Challenges and future perspectives

Photocatalytic water splitting for the creation of H_2 has several fundamental drawbacks that make it unsuitable for practical and industrial use. Water resource plays a significant role as well; natural water sources, such as seawater or wastewater, often contain impurities like salts, organic matter, or heavy metals that can poison the photocatalyst surface or compete with water-splitting reactions, necessitating pre-treatment processes [159]. In addition, the world's widespread access to solar and ocean resources allows for greater geographic flexibility and lessens dependency on the existing scarcity of freshwater supplies [160]. The complicated nature of saltwater and the photocatalyst's high sensitivity, however, mean that Seawater splitting using direct photocatalysis for H_2 synthesis still exhibits a low effectiveness [85].

One of the main challenges is low quantum efficiency since most photocatalysts are confined to the absorption of UV light, which accounts for only around four to five% of the electromagnetic spectrum of the sun, abandoning an enormous amount of visible and infrared energy unutilized [15, 16]. Furthermore, electron-hole recombination happens immediately in most photocatalysts, significantly lowering charge separation efficiency and, consequently, hydrogen production. Some of the challenges stated as the sun releases radiation ranging from an X-ray to radio waves, although most of the strong radiation is found in the visible spectrum, accounting for 43% of the total solar energy that reaches Earth [16]. The splitting of water without a photocatalyst uses just (UV) radiation up to 400 nm with entirely quantum efficiency [161]. However, the (STH) has an energy transformation efficiency of about 2%. By extending the photocatalyst's absorption zone to 700 and 1000 nm, STH efficiency may be increased by 25% and 45%, respectively. However, using a semiconductor-based photocatalyst in an environment with 650 nm light results in a conversion efficiency of less than 60% from solar to hydrogen. Researchers investigated several single photocatalysts for water splitting. They discovered that 80% of them had only been active under (UV visible light), which represents only 4–8% of solar light [148].

The individual photocatalysts activity is drastically reduced due to the high rate of electron/hole recombination [162, 163]. More consideration should be given to the theory that photocatalytic activity can be increased by blocking recombination. Several strategies for modification have been introduced to overcome the challenges mentioned above. The absorption and light source are considerably increased when plasma exciton elements and up-conversion processes are incorporated into photocatalytic materials. It has significant implications for the creation of new, effective photocatalysts with broad-spectrum absorption capabilities. Furthermore, complexation can be avoided mainly by controlling shape and metal doping. These techniques, which can significantly improve photocatalytic performance, use photocatalytic effects and create heterojunctions between semiconductors to build external circuits [164–166].

The bandgap energy of photocatalysts presents a dual challenge: while narrower bandgaps can absorb more sunlight, they often lack the redox potential necessary to drive water splitting, whereas wider bandgaps restrict absorption to UV light. The oxygen evolution reaction (OER), a critical part of water splitting, is particularly challenging due to its slow kinetics and high overpotential requirements, which limit the overall process efficiency [167, 168]. Furthermore, several systems rely on sacrificial agents (e.g., methanol or ethanol) to improve reaction rates and reduce recombination, but these additives compromise the sustainability and scalability of the technology. Along with cited findings and references, the crucial factors influencing photocatalyst performance have been thoroughly examined. The results show that the type of water resource used, whether pure water or seawater, affects the process due to impurities and competing reactions. Pure water offers a controlled environment, while seawater introduces ions and organic matter that may require pre-treatment or specialized photocatalysts to handle their complexity. Careful control and optimization of these parameters are essential for achieving high hydrogen yields and sustainable water-splitting processes. Its constituent elements and band structure determine the photocatalyst's synthesis method [169, 170].

The synthesis method used to prepare the photocatalyst is vital for determining its structural, optical, and electronic properties. Techniques such as hydrothermal, solvothermal, sol-gel, and doping can tailor features like particle size, crystallinity, and bandgap to improve hydrogen production efficiency. The substrate's pH regulates the catalyst-substrate interfacial chemistry. Neutral pH (7) is often used, but the optimal pH can vary based on the conditions of the reaction and type of catalyst. Adjusting the catalyst's surface charge and reactants and products adsorption both are impacted by pH [171–173].

The light source and the irradiation intensity control the number of e^-/h^+ pairs produced. Typically, a 300-watt (UV) xenon light is used, with the optimal wavelength range depending on the bandgap of the photocatalyst. The amount of light absorbed is reduced by the excessive use of catalyst can cause incident light to scatter and become blocked, which limits the quantity of catalyst loading into the system. Thermal management is another issue, as elevated temperatures can improve reaction kinetics but may destabilize the photocatalyst or lead to unwanted side reactions [174] study looked at how the reaction temperature affected the photocatalytic efficiency of TiO_2 with Pd and Cu cocatalysts [175].

The quantum effect, or electron-hole separation and recombination, is largely impacted by reaction temperature. The reactivity of TiO_2 and Pd/TiO_2 increased as the

reaction temperature rose from 0 to 50 °C. However, at 70 °C, the reaction rate for TiO_2 dropped slightly, reducing the effectiveness of Pd/TiO_2. In contrast, Cu/TiO_2 showed the highest activity at room temperature compared to other temperatures. When comparing the reaction rates under ideal conditions, Pd/TiO_2 demonstrated significantly higher catalytic efficiency than Cu/TiO_2, while Cu/TiO_2 performed slightly better than TiO_2. The effect of temperature on the catalyst's activity depends on the type of cocatalyst used. At temperatures above 70 °C, the recombination of charge carriers becomes more prominent, reducing efficiency. The optimal temperature range for photolysis of organic materials is between 50 °C and 80 °C [114, 121].

The catalyst loading significantly impacts light absorption and photocatalytic efficiency. Using too little catalyst results in insufficient active sites, while excessive amounts can block light penetration and lead to scattering, reducing overall performance. Lastly, the presence of dissolved oxygen plays a dual role in photocatalytic water splitting, acts as an electron scavenger to decrease the recombination of charge carriers, excessive oxygen can compete with hydrogen production reactions, lowering efficiency [176, 177]. Typically, a low dissolved oxygen concentration is desired to minimize the recombination of electron-hole pairs. Purging systems with inert gas like nitrogen or argon can help reduce oxygen levels [178]. Finally, the scalability and economic viability of photocatalytic systems remain a challenge due to the high cost of synthesis techniques like doping, heterostructure fabrication, or nanostructuring, combined with the difficulty of implementing these methods on a large scale. These challenges underscore the need for continued research into cost-effective, stable, and efficient photocatalysts, as well as innovations in reactor design and water treatment technologies.

5 Conclusion

This review comprehensively addresses the essential aspects of photocatalytic hydrogen production via water splitting, including theoretical background, efficient mechanisms, and the influence of critical operational parameters. From the discussion, several major challenges and future research directions emerge as follows:

Challenges and Emerging Strategies for Seawater Photocatalytic Hydrogen Production.

Limited visible-light utilization.

Limited visible-light utilization remains a major bottleneck in seawater photocatalysis and is being addressed through band-gap engineering, plasmonic sensitization, and Z-/S-scheme heterojunctions that enhance solar absorption while maintaining sufficient redox potentials in saline environments.

Catalyst instability caused by Cl^- and multivalent ions.

Catalyst instability induced by aggressive ions such as Cl^-, Mg^{2+}, and Ca^{2+} has driven the development of chlorine-resistant coatings, halide-tolerant materials, and protective encapsulation strategies to suppress photocorrosion and surface passivation.

Fast charge recombination in seawater.

Fast charge recombination, often exacerbated by high ionic strength, is being mitigated via heterojunction construction, cocatalyst loading, defect engineering, and photothermal-assisted systems that promote efficient charge separation and transfer.

Surface fouling and catalyst deactivation.

Surface fouling and catalyst deactivation caused by salt precipitation and biofouling highlight the need for anti-fouling surface modifications and functional coatings that preserve active sites and light penetration.

Competing chlorine evolution and ROS formation.

Competing chlorine evolution and reactive oxygen species (ROS) formation necessitate selective cocatalysts and reaction-pathway engineering to favor proton reduction over parasitic oxidation reactions, ensuring safer and more efficient hydrogen generation.

Outlook:

Addressing these challenges through targeted material innovation, interface engineering, and seawater-specific reactor optimization will be essential to achieving scalable, stable, and economically viable photocatalytic hydrogen production. By advancing these research directions, photocatalytic seawater splitting can progress from laboratory feasibility to practical renewable hydrogen generation, contributing significantly to global clean energy strategies.

Author contributions

Shaiza Asif (Write the main manuscript, Conceptualization, Writing, Reviewing, and Editing)Khairul Anwar Mohammad Bin Said (Supervision, Writing, Reviewing, and Editing) Nadeem A Khan (Investigation)Imtiyaz Akbar Najar (Writing, Reviewing and Editing)Md Rezaur Rahman (Writing, Reviewing, and Editing)Kelvin Kuok King Kuok (Writing, Reviewing, and Editing).

Funding

Open Access funding provided by Universiti Malaysia Sarawak. The authors would like to express our gratitude to the Sarawak Research and Development Council (SRDC) for the Research Initiation Fund IRG/F02/SRDC/86331/2024. We also would like to acknowledge the Research and Innovation Management Centre (RIEC) of the University Malaysia Sarawak for their supporting role in managing research activities.

Data availability

The data supporting the findings of this study are available from corresponding author upon request.

Declarations

Ethics approval

Not applicable.

Consent to Participate

Not applicable.

Consent to Publish

Not applicable.

Competing interests

The authors declare no competing interests.

Received: 11 September 2025 / Accepted: 2 March 2026

Published online: 13 March 2026

References

1. Zha E, et al. Depth-dependent mechanical-seepage behavior and safety mining distance of the steeply inclined coal mine underground reservoir. Int J Min Sci Technol. 2025. https://doi.org/10.1016/j.ijmst.2025.07.006.
2. Lei M, Zhao J, Dong H, Wang Z. Gel-sol transition process of waxy crude oil under different engineering methods. Fuel. 2026;404:136298. https://doi.org/10.1016/j.fuel.2025.136298.
3. Qiu B, Chen R, Lv H, Zhu J, Li Y. Research on adaptability of simulation state equation of hydrogen-blended natural gas pipeline. J Pipeline Sci Eng. 2025;100346. https://doi.org/10.1016/j.jpse.2025.100346.
4. Shaheen F, et al. Chapter 20 - Oleaginous microbes for biodiesel production using lignocellulosic biomass as feedstock. In: Shah MP, editor. Green Approach to Alternative Fuel for a Sustainable Future. Elsevier; 2023. pp. 271–96. https://doi.org/10.1016/B978-0-12-824318-3.00020-5.
5. Segovia-Hernández JG, Hernández S, Cossío-Vargas E, Sánchez-Ramírez E. Tackling sustainability challenges in Latin America and Caribbean from the chemical engineering perspective: a literature review in the last 25 years. Chem Eng Res Des. 2022;188:483–527. https://doi.org/10.1016/j.cherd.2022.10.012.
6. Mutezo G, Mulopo J. A review of Africa's transition from fossil fuels to renewable energy using circular economy principles. Renew Sustain Energy Rev. 2021;137:110609. https://doi.org/10.1016/j.rser.2020.110609.

7. Acar C, Dincer I. 3.22 - Hydrogen production. In: Dincer I, editor. Comprehensive Energy Systems (Second Edition). Oxford: Elsevier; 2025. p. 196–248. https://doi.org/10.1016/B978-0-44-313219-3.00024-1.
8. Schulthoff M, Rudnick I, Bose A, Gençer E. Role of hydrogen in a low-carbon electric power system: a case study. Front Energy Res. 2021;8:585461.
9. French S. The role of zero and low carbon hydrogen in enabling the energy transition and the path to net zero greenhouse gas emissions: With global policies and demonstration projects hydrogen can play a role in a net zero future. Johns Matthey Technol Rev. 2020;64(3):357–70.
10. Hosseini SE. Hydrogen diplomacy. Future Publishing LLC; 2024.
11. Noussan M, Raimondi PP, Scita R, Hafner M. The role of green and blue hydrogen in the energy transition—a technological and geopolitical perspective. Sustainability. 2020;13(1):298.
12. Ameta R, Solanki MS, Benjamin S, Ameta SC. Photocatalysis. In: Advanced oxidation processes for waste water treatment. Elsevier; 2018. p. 135–75.
13. Banerjee S, Pillai SC, Falaras P, O'Shea KE, Byrne JA, Dionysiou DD. New insights into the mechanism of visible light photocatalysis. J Phys Chem Lett. 2014;5(15):2543–54. https://doi.org/10.1021/jz501030x.
14. Zhang L, Kuang P, Yu J. Introductory chapter: Fundamentals of photocatalysis and electrocatalysis. In: Graphene Oxide-Metal Oxide and Other Graphene Oxide-Based Composites in Photocatalysis and Electrocatalysis. Elsevier; 2022. p. 1–30.
15. Peiris S, de Silva HB, Ranasinghe KN, Bandara SV, Perera IR. Recent development and future prospects of TiO2 photocatalysis. J Chin Chem Soc. 2021;68(5):738–69.
16. Ahmad R, Ahmad Z, Khan AU, Mastoi NR, Aslam M, Kim J. Photocatalytic systems as an advanced environmental remediation: recent developments, limitations and new avenues for applications. J Environ Chem Eng. 2016;4(4):4143–64.
17. Qu K-G, et al. Covalent organic framework assisted low-content ultrafine Ru on porous N-doped carbon for efficient hydrogen evolution reaction. Rare Met. 2025;44(3):2094–102.
18. Yakub I, Mohamad Said KA, Baini R, Mohamed Amin MA. Enhancing the catalytic properties of a biochar-supported copper oxide in nitric oxide selective reduction with hydrogen. Braz J Chem Eng. 2025;42(2):623–35.
19. Reasad M, Sumaiya S, Rahman Khan MA. Nanomaterial-enhanced composite membranes for sustainable water treatment: advances, challenges, and future prospects. Int J Energy Water Resour. 2025;10(1):31. https://doi.org/10.1007/s42108-025-00457-6.
20. Kudo A, Miseki Y. Heterogeneous photocatalyst materials for water splitting. Chem Soc Rev. 2009;38(1):253–78. https://doi.org/10.1039/b800489g.
21. Kim JH, Hansora D, Sharma P, Jang JW, Lee JS. Toward practical solar hydrogen production-an artificial photosynthetic leaf-to-farm challenge. Chem Soc Rev. 2019;48(7):1908–71. https://doi.org/10.1039/c8cs00699g.
22. Ismail AA, Bahnemann DW. Photochemical splitting of water for hydrogen production by photocatalysis: a review. Sol Energy Mater Sol Cells. 2014;128:85–101. https://doi.org/10.1016/j.solmat.2014.04.037.
23. Zhou H, Yan R, Zhang D, Fan T. Challenges and perspectives in designing artificial photosynthetic systems. Chem Eur J. 2016;22(29):9870–85. https://doi.org/10.1002/chem.201600289.
24. Jafari T, Moharreri E, Amin AS, Miao R, Song W, Suib SL. Photocatalytic water splitting - the untamed dream: a review of recent advances. Molecules. 2016. https://doi.org/10.3390/molecules21070900.
25. Tong H, Ouyang S, Bi Y, Umezawa N, Oshikiri M, Ye J. Nano-photocatalytic materials: possibilities and challenges. Adv Mater. 2012;24(2):229–51.
26. Linsebigler AL, Lu G, Yates JT Jr. Photocatalysis on TiO2 surfaces: principles, mechanisms, and selected results. Chem Rev. 1995;95(3):735–58.
27. Abe R. Recent progress on photocatalytic and photoelectrochemical water splitting under visible light irradiation. J Photochem Photobiol C Photochem Rev. 2010;11(4):179–209. https://doi.org/10.1016/j.jphotochemrev.2011.02.003.
28. Chen X, Shen S, Guo L, Mao SS. Semiconductor-based photocatalytic hydrogen generation. Chem Rev. 2010;110(11):6503–70.
29. Mohammed Y, Hafeez HY, Mohammed J, Suleiman AB, Ndikilar CE, Idris MG. Hydrogen production via photocatalytic water splitting using spinel ferrite-based photocatalysts: recent and future perspectives. Next Energy. 2024;4:100145. https://doi.org/10.1016/j.nxener.2024.100145.
30. Hamdani IR, Bhaskarwar AN. Recent progress in material selection and device designs for photoelectrochemical water-splitting. Renew Sustain Energy Rev. 2021;138:110503. https://doi.org/10.1016/j.rser.2020.110503.
31. Rozhkova EA, Ariga K. From molecules to materials. Springer; 2015.
32. Aresta M, Dibenedetto A, Macyk W. Hybrid (Enzymatic and Photocatalytic) Systems for CO 2-Water Coprocessing to Afford Energy-Rich Molecules. In: From Molecules to Materials: Pathways to Artificial Photosynthesis. 2015. p. 149–69.
33. Zaleska-Medynska A. Metal oxide-based photocatalysis: fundamentals and prospects for application. Elsevier; 2018.
34. Kageshima Y, et al. Photocatalytic and photoelectrochemical hydrogen evolution from water over Cu2Sn x Ge1−x S3 particles. J Am Chem Soc. 2021;143(15):5698–708.
35. Serpone N, et al. Standardization protocol of process efficiencies and activation parameters in heterogeneous photocatalysis: relative photonic efficiencies ζr. J Photochem Photobiol A Chem. 1996;94(2):191–203. https://doi.org/10.1016/1010-6030(95)04223-7.
36. Shi Y, et al. Boosting photothermal-assisted photocatalytic water/seawater splitting into hydrogen based on greenhouse-induced photothermal effect. J Colloid Interface Sci. 2024;653:1339–47. https://doi.org/10.1016/j.jcis.2023.09.170.
37. Lu J, et al. Construction of S-scheme heterojunction catalytic nanoreactor for boosted photothermal-assisted photocatalytic H2 production. Appl Surf Sci. 2024;642:158648. https://doi.org/10.1016/j.apsusc.2023.158648.
38. Shi Y, Li L, Xu Z, Guo F, Shi W. Construction of full solar-spectrum available S-scheme heterojunction for boosted photothermal-assisted photocatalytic H2 production. Chem Eng J. 2023;459:141549. https://doi.org/10.1016/j.cej.2023.141549.
39. Zakaria H, et al. A novel TiO2-x/TiN@ACB composite for synchronous photocatalytic Cr(VI) reduction and water photothermal evaporation under visible/infrared light illumination. Chemosphere. 2023;311:137137. https://doi.org/10.1016/j.chemosphere.2022.137137.
40. Merabet N, Kerboua K. Sonolytic and ultrasound-assisted techniques for hydrogen production: a review based on the role of ultrasound. Int J Hydrogen Energy. 2022;47(41):17879–93.
41. Harada H. Sonophotocatalytic decomposition of water using TiO2 photocatalyst. Ultrason Sonochem. 2001;8(1):55–8.

42. Moradi S, Rodriguez-Seco C, Hayati F, Ma D. Sonophotocatalysis with photoactive nanomaterials for wastewater treatment and bacteria disinfection. ACS Nanosci Au. 2023;3(2):103–29.
43. Soni S et al. 'Recent advances in metal (M = Ni/Fe/Cu/Zn) oxide nanomaterials-mediated removal of dyes from wastewater'. J Taiwan Inst Chem Eng, 2024 vol166 (2) . 105565. https://doi.org/10.1016/j.jtice.2024.105565
44. Cotana F, Rossi F, Urbani M. 'Study of water photosonolysis for hydrogen production', in 3rd Int Green Energy Conf, Citeseer, 2007; pp. 3–8.
45. He H-Y. Metallic WSe2: Sn nanosheets assembled on graphene by a modified hydrothermal process for hydrogen evolution reaction. Colloids Surf A Physicochem Eng Asp. 2020;589:124149. https://doi.org/10.1016/j.colsurfa.2019.124149.
46. Hayashi H, Hakuta Y. Hydrothermal synthesis of metal oxide nanoparticles in supercritical water. Materials. 2010;3(7):3794–817.
47. Zhang Z-G, et al. One-step low temperature hydrothermal synthesis of flexible TiO2/PVDF@MoS2 core-shell heterostructured fibers for visible-light-driven photocatalysis and self-cleaning. Nanomaterials. 2019. https://doi.org/10.3390/nano9030431.
48. Lv S, et al. Graphene oxide coupled high-index facets CdZnS with rich sulfur vacancies for synergistic boosting visible-light-catalytic hydrogen evolution in natural seawater: experimental and DFT study. J Colloid Interface Sci. 2022;623:34–43.
49. Cheng Z, Zhang X, Bo C, Sun Y, Li C, Piao L. Precise design of TiO2 photocatalyst for efficient photocatalytic H2 production from seawater splitting. Int J Hydrogen Energy. 2024;55:542–9. https://doi.org/10.1016/j.ijhydene.2023.11.211.
50. Zhang J, Lei Y, Cao S, Hu W, Piao L, Chen X. Photocatalytic hydrogen production from seawater under full solar spectrum without sacrificial reagents using TiO2 nanoparticles. Nano Res. 2022;15(3):2013–22.
51. Ng B-J, et al. Heteroatom P filling activates intrinsic S atomic sites of few-layered ZnIn 2 S 4 via modulation of H adsorption kinetics for sacrificial agent-free photocatalytic hydrogen evolution from pure water and seawater. J Mater Chem A. 2023;11(32):17079–90.
52. Li Y, Gao C, Long R, Xiong Y. Photocatalyst design based on two-dimensional materials. Mater Today Chem. 2019;11:197–216. https://doi.org/10.1016/j.mtchem.2018.11.002.
53. Qin H, et al. Spinel ferrites (MFe2O4): synthesis, improvement and catalytic application in environment and energy field. Adv Colloid Interface Sci. 2021;294:102486. https://doi.org/10.1016/j.cis.2021.102486.
54. Grushevskaya S, Belyanskaya I, Kozaderov O. Approaches for modifying oxide-semiconductor materials to increase the efficiency of photocatalytic water splitting. Materials. 2022. https://doi.org/10.3390/ma15144915.
55. Yang G, Chen T, Liu H, Xing C, Yu G, Li X. Bi-doped twin crystal Zn0. 5Cd0. 5S photocatalyst for highly efficient photocatalytic hydrogen production from water. Appl Surf Sci. 2023;616:156393.
56. He Y, Zhang J, Rong J, Mei J, Liang Q, Li Z. Triptycene-based polymer-incorporated Cd x Zn1−x S nanorod with enhanced interfacial charge transfer for stable photocatalytic hydrogen production in seawater. Inorg Chem. 2023;62(17):6833–42.
57. Park Y-K, Kim B-J, Jeong S, Jeon K-J, Chung K-H, Jung S-C. Characteristics of hydrogen production by photocatalytic water splitting using liquid phase plasma over Ag-doped TiO2 photocatalysts. Environ Res. 2020;188:109630. https://doi.org/10.1016/j.envres.2020.109630.
58. Giannakas AE, Seristatidou E, Deligiannakis Y, Konstantinou I. Photocatalytic activity of N-doped and N–F co-doped TiO2 and reduction of chromium(VI) in aqueous solution: an EPR study. Appl Catal B. 2013;132:460–8. https://doi.org/10.1016/j.apcatb.2012.12.017.
59. González CMO, Morales EMC, de M. N. Tellez A, Quezada TES, Kharissova OV, Méndez-Rojas MA. Chapter 18 - CO2 capture by MOFs. In: Kharisov B, Kharissova O-H, editors. Handbook of greener synthesis of nanomaterials and compounds. Elsevier; 2021. p. 407–48. https://doi.org/10.1016/B978-0-12-822446-5.00018-6.
60. Sun H, Shi Y, Shi W, Guo F. High-crystalline/amorphous g-C3N4 S-scheme homojunction for boosted photocatalytic H2 production in water/simulated seawater: interfacial charge transfer and mechanism insight. Appl Surf Sci. 2022;593:153281.
61. Han Y, Dong X. Mn0. 3Cd0. 7S nanorods modified by amorphous FexP with improved photocatalytic activity and stability for H2 evolution. Catal Lett. 2022;152(6):1660–8.
62. Zhu Y, Han Q, Zhou Y. Synergistic selenium vacancies and bismuth metal centers on Bi 2 Se 3 for enhanced photocatalytic CO 2 reduction. Nanoscale Adv. 2025;7(20):6640–5.
63. Zhao L, et al. Engineering Co single atoms in ultrathin BiOCl nanosheets for boosted CO2 photoreduction. Adv Funct Mater. 2025;35(9):2416346. https://doi.org/10.1002/adfm.202416346.
64. Gou J, Zhuge J, Liang F. 4 - Processing of polymer nanocomposites. In: Advani SG, Hsiao K-TBT-MTfPMC(P, editors. Woodhead Publishing Series in Composites Science and Engineering. Woodhead Publishing; 2012. p. 95–119. https://doi.org/10.1533/9780857096258.1.95.
65. Mumtaz F, et al. Optimization of z-scheme Bi0.5Na0.5TiO3/RGO-Co3O4 composite catalyst for water splitting reaction through piezo-photocatalysis. Int J Hydrogen Energy. 2024;78:1468–80. https://doi.org/10.1016/j.ijhydene.2024.06.387.
66. Guo M, Chen M, Xu J, Wang C, Wang L. C, N-vacancies and Br dopant co-enhanced photocatalytic H2 evolution of g-C3N4 from water and simulated seawater splitting. Chem Eng J. 2023;461:142046.
67. Magero D, Mestiri T, Alimi K, Casida ME. 5 - Computational studies of ruthenium and iridium complexes for energy sciences and progress on greener alternatives. In: Mammino L-G, editor. Advances in Green and Sustainable Chemistry. Elsevier; 2022. p. 115–45. https://doi.org/10.1016/B978-0-12-819879-7.00042-8.
68. Politzer P, Murray J, Yepes D, Jaque P. Driving and retarding forces in a chemical reaction. J Mol Model. 2014;20:2351. https://doi.org/10.1007/s00894-014-2351-0.
69. Onsuratoom S, Chavadej S, Sreethawong T. Hydrogen production from water splitting under UV light irradiation over Ag-loaded mesoporous-assembled TiO2–ZrO2 mixed oxide nanocrystal photocatalysts. Int J Hydrogen Energy. 2011;36(9):5246–61. https://doi.org/10.1016/j.ijhydene.2011.01.176.
70. Cheng C, Zhang J, Zeng R, Xing F, Huang C. Schottky barrier tuning via surface plasmon and vacancies for enhanced photocatalytic H2 evolution in seawater. Appl Catal B. 2022;310:121321. https://doi.org/10.1016/j.apcatb.2022.121321.
71. Pierre A. Introduction to Sol-Gel Processing. 2020. https://doi.org/10.1007/978-3-030-38144-8
72. Dholam R, Patel N, Adami M, Miotello A. Hydrogen production by photocatalytic water-splitting using Cr-or Fe-doped TiO2 composite thin films photocatalyst. Int J Hydrogen Energy. 2009;34(13):5337–46.
73. Li X, Yu J, Wageh S, Al-Ghamdi AA, Xie J. Graphene in photocatalysis: a review. small. 2016;12(48):6640–96.

74. Xiang Q, Yu J, Jaroniec M. Graphene-based semiconductor photocatalysts. Chem Soc Rev. 2012;41(2):782–96.
75. Low J, Yu J, Jaroniec M, Wageh S, Al-Ghamdi AA. Heterojunction photocatalysts. Adv Mater. 2017;29(20):1601694.
76. Machín A et al. 'Biomimetic catalysts based on Au@ ZnO–graphene composites for the generation of hydrogen by water splitting', Biomim. 2020;5(3):39.
77. Ma S, Wang W. 'Preparation and photocatalytic hydrogen evolution of g-C3N4/ZnO composite', E3S Web of Conf. 2020;165:05007. https://doi.org/10.1051/e3sconf/202016505007
78. Girish YR, et al. Rapid and facile synthesis of Z-scheme ZnO/g-C3N4 heterostructure as efficient visible light-driven photocatalysts for dye degradation and hydrogen evolution reaction. J Hazard Mater Adv. 2023;9:100230. https://doi.org/10.1016/j.hazadv.2023.100230.
79. Kumar V, et al. Nanocomposite marvels: unveiling breakthroughs in photocatalytic water splitting for enhanced hydrogen evolution. ACS Omega. 2024;9(6):6147–64. https://doi.org/10.1021/acsomega.3c07822.
80. Zhao T, Wang Q, Du A. High piezo-photocatalytic efficiency of H2 production by CuS/ZnO nanostructure under solar and ultrasonic exposure. Mater Lett. 2021;294:129752.
81. Gotipamul P, Maheswaran R, Pandiaraj S, Alqarni SA, Chidambaram S. Piezo-photocatalytically enhanced H2 production and pollutant removal from ZnO nanorods grown on g-C3N4 layers. Materials Today Sustainability. 2023;24:100501. https://doi.org/10.1016/j.mtsust.2023.100501.
82. Wei Y, Shahid MZ, Lyu S, Sun W, Lyu S. One-pot, ligand-free, room-temperature synthesis of Au/Pd/ZnO nanoclusters with ultra-low noble metal loading and synergistically improved photocatalytic performances. RSC Adv. 2021;11(37):22618–24.
83. Kumar S, Kumar A, Kumar A, Krishnan V. Nanoscale zinc oxide based heterojunctions as visible light active photocatalysts for hydrogen energy and environmental remediation. Catal Rev. 2020;62(3):346–405.
84. Huo J, Fang L, Lei Y, Zeng G, Zeng H. Facile preparation of yttrium and aluminum co-doped ZnO via a sol–gel route for photocatalytic hydrogen production. J Mater Chem Mater. 2014;2(29):11040–4.
85. Dresp S, Dionigi F, Klingenhof M, Strasser P. Direct electrolytic splitting of seawater: opportunities and challenges. ACS Energy Lett. 2019;4(4):933–42.
86. Zhang J, Hu W, Cao S, Piao L. Recent progress for hydrogen production by photocatalytic natural or simulated seawater splitting. Nano Res. 2020;13:2313–22.
87. Ng KH, Lai SY, Cheng CK, Cheng YW, Chong CC. Photocatalytic water splitting for solving energy crisis: myth, fact or busted? Chem Eng J. 2021;417:128847.
88. Dang V-H, Nguyen T-A, Le M-V, Nguyen DQ, Wang YH, Wu J-S. Photocatalytic hydrogen production from seawater splitting: current status, challenges, strategies and prospective applications. Chem Eng J. 2024. https://doi.org/10.1016/j.cej.2024.149213.
89. Pelayo D, Pérez-Peña E, Rivero MJ, Ortiz I. Shedding light on the photocatalytic hydrogen generation from seawater using CdS. Catal Today. 2024;433:114672. https://doi.org/10.1016/j.cattod.2024.114672.
90. Shanmugaratnam S, Ravirajan P, Shivatharsiny Y, Velauthapillai D. Green hydrogen production through photocatalytic seawater splitting on MS2/TiO2 (M = Ni/Co/Sn) nanocomposites over simulated solar irradiation. Int J Hydrogen Energy. 2024;91:673–82. https://doi.org/10.1016/j.ijhydene.2024.10.091.
91. Lin Y-R, Chang Y-C, Ko F-H. One-pot microwave-assisted synthesis of In2S3/In2O3 nanosheets as highly active visible light photocatalysts for seawater splitting. Int J Hydrogen Energy. 2024;52:953–63.
92. Jiang Y, et al. Efficient and stable piezo-photocatalytic splitting of water and seawater by interfacial engineering of Na0.5Bi0.5TiO3/Na0.5Bi4.5Ti4O15 self-generated heterojunctions. Nano Energy. 2023;116:108830. https://doi.org/10.1016/j.nanoen.2023.108830.
93. Xia L, Lu Y, Li Y-Z, Hu Z-Y, Yang X-Y. TiO2-rGO-Cu complex: a photocatalyst possessing an interfacial electron transport mechanism to enhance hydrogen production from seawater. Chem Phys Lett. 2023;822:140498.
94. Xiong G, et al. Well-defined Z-scheme Na2Ti3O7/Ag/CdS multidimensional heterojunctions with enhanced H2 production from seawater under visible light. Int J Hydrogen Energy. 2022;47(71):30503–16. https://doi.org/10.1016/j.ijhydene.2022.07.031.
95. Van Dang H, Wang YH, Wu JCS. Exploration of photocatalytic seawater splitting on Pt/GaP-C3N4 under simulated sunlight. Appl Surf Sci. 2022;572:151346. https://doi.org/10.1016/j.apsusc.2021.151346.
96. Guo F, et al. A ragged porous hollow tubular carbon nitride towards boosting visible-light photocatalytic hydrogen production in water and seawater. Renew Energy. 2022;188:1–10. https://doi.org/10.1016/j.renene.2022.01.107.
97. Bastos SAL, Lopes PAL, Santos FN, Silva LA. Experimental design as a tool to study the reaction parameters in hydrogen production from photoinduced reforming of glycerol over CdS photocatalyst. Int J Hydrogen Energy. 2014;39(27):14588–95. https://doi.org/10.1016/j.ijhydene.2014.07.073.
98. Jiang X, Fu X, Zhang L, Meng S, Chen S. Photocatalytic reforming of glycerol for H2 evolution on Pt/TiO2: fundamental understanding the effect of co-catalyst Pt and the Pt deposition route. J Mater Chem. 2015;3(5):2271–82. https://doi.org/10.1039/c4ta06052k.
99. Loosli F, Coustumer PL, Stoll S. TiO2 nanoparticles aggregation and disaggregation in presence of alginate and Suwannee River humic acids. pH and concentration effects on nanoparticle stability. Water Res. 2013;47(16):6052–63. https://doi.org/10.1016/j.watres.2013.07.021.
100. Malato S, Fernández-Ibáñez P, Maldonado MI, Blanco J, Gernjak W. Decontamination and disinfection of water by solar photocatalysis: recent overview and trends. Catal Today. 2009;147(1):1–59. https://doi.org/10.1016/j.cattod.2009.06.018.
101. Yurdakal S, et al. Optical properties of TiO2 suspensions: influence of pH and powder concentration on mean particle size. Ind Eng Chem Res. 2007;46(23):7620–6.
102. Hamid S, Ivanova I, Jeon TH, Dillert R, Choi W, Bahnemann DW. Photocatalytic conversion of acetate into molecular hydrogen and hydrocarbons over Pt/TiO2: pH dependent formation of Kolbe and Hofer-Moest products. J Catal. 2017;349:128–35. https://doi.org/10.1016/j.jcat.2017.02.033.
103. Wang P, Guan Z, Li Q, Yang J. Efficient visible-light-driven photocatalytic hydrogen production from water by using Eosin Y-sensitized novel g-C3N4/Pt/GO composites. J Mater Sci. 2018;53(1):774–86. https://doi.org/10.1007/s10853-017-1540-5.
104. Wang G, et al. Highly efficient visible-light driven photocatalytic hydrogen production from a novel Z-scheme Er3+:YAlO3/Ta2O5-V5+||Fe3+-TiO2/Au coated composite. J Power Sources. 2018;373:161–71. https://doi.org/10.1016/j.jpowsour.2017.11.005.

105. Pellegrino F, et al. Influence of agglomeration and aggregation on the photocatalytic activity of TiO2 nanoparticles. Appl Catal B. 2017;216:80–7.
106. Di Paola A, Ikeda S, Marcì G, Ohtani B, Palmisano L. Transition metal doped TiO2: physical properties and photocatalytic behaviour. Int J Photoenergy. 2001;3(4):171–6.
107. Zhou J, Zhang Y, Zhao XS, Ray AK. Photodegradation of benzoic acid over metal-doped TiO2. Ind Eng Chem Res. 2006;45(10):3503–11. https://doi.org/10.1021/ie051098z.
108. Di Paola A, Garćia-López E, Ikeda S, Marcì G, Ohtani B, Palmisano L. Photocatalytic degradation of organic compounds in aqueous systems by transition metal doped polycrystalline TiO2. Catal Today. 2002;75(1):87–93. https://doi.org/10.1016/S0920-5861(02)00048-2.
109. Li M, Li Y, Peng S, Lu G, Li S. Photocatalytic hydrogen generation using glycerol wastewater over Pt/TiO2. Front Chem China. 2009;4(1):32–8. https://doi.org/10.1007/s11458-009-0019-6.
110. Fujita S, Kawamori H, Honda D, Yoshida H, Arai M. Photocatalytic hydrogen production from aqueous glycerol solution using NiO/TiO2 catalysts: effects of preparation and reaction conditions. Appl Catal B Environ. 2016;181:818–24. https://doi.org/10.1016/j.apcatb.2015.08.048.
111. Clugston M, Flemming R. Advanced chemistry. Oxford University Press; 2000.
112. Karimi Estahbanati MR, Mahinpey N, Feilizadeh M, Attar F, Iliuta MC. Kinetic study of the effects of pH on the photocatalytic hydrogen production from alcohols. Int J Hydrogen Energy. 2019;44(60):32030–41. https://doi.org/10.1016/j.ijhydene.2019.10.114.
113. Nasikhudin M, Diantoro A, Kusumaatmaja, Triyana K. 'Study on photocatalytic properties of TiO2 nanoparticle in various pH condition', in J Phys: Conf Ser, IOP Publishing, 2018. p. 12069.
114. Guan X, Chowdhury FA, Pant N, Guo L, Vayssieres L, Mi Z. Efficient unassisted overall photocatalytic seawater splitting on GaN-based nanowire arrays. J Phys Chem C. 2018;122(25):13797–802. https://doi.org/10.1021/acs.jpcc.8b00875.
115. Vequizo JJM, Matsunaga H, Ishiku T, Kamimura S, Ohno T, Yamakata A. Trapping-induced enhancement of photocatalytic activity on brookite TiO2 powders: comparison with anatase and rutile TiO2 powders. ACS Catal. 2017;7(4):2644–51.
116. Maeda K, Teramura K, Domen K. Effect of post-calcination on photocatalytic activity of (Ga1 − xZnx)(N1 − xOx) solid solution for overall water splitting under visible light. J Catal. 2008;254(2):198–204.
117. Bodzek M, Rajca M. Photocatalysis in the treatment and disinfection of water. Part I. Theoretical backgrounds/Fotokataliza w oczyszczaniu i dezynfekcji wody część i. podstawy teoretyczne. Ecol Chem Eng S. 2012;19(4):489–512.
118. Herrmann J-M, Puzenat E. 'Photocatalytic engineering', Green Process Engineering: From Concepts to Industrial Appl. 2015. p. 364.
119. Thiruvenkatachari R, Vigneswaran S, Moon IS. A review on UV/TiO 2 photocatalytic oxidation process (Journal Review). Korean J Chem Eng. 2008;25:64–72.
120. Chen D, Ray AK. Photodegradation kinetics of 4-nitrophenol in TiO_2 suspension. Water Res. 1998;32(11):3223–34.
121. Mozia S, Tomaszewska M, Morawski AW. Photocatalytic degradation of azo-dye Acid Red 18. Desalination. 2005;185(1–3):449–56.
122. Rincón A-G, Pulgarin C. Comparative evaluation of Fe3 + and TiO_2 photoassisted processes in solar photocatalytic disinfection of water. Appl Catal B. 2006;63:3–4.
123. Dalrymple OK, Stefanakos E, Trotz MA, Goswami DY. A review of the mechanisms and modeling of photocatalytic disinfection. Appl Catal B. 2010;98:1–2.
124. Chong MN, Jin B, Chow CWK, Saint C. Recent developments in photocatalytic water treatment technology: a review. Water Res. 2010;44(10):2997–3027.
125. Mozia S, Morawski AW, Toyoda M. The influence of solution composition on the effectiveness of degradation of ibuprofen sodium salt in a hybrid photocatalysis–membrane distillation system. J Adv Oxid Technol. 2012;15(1):21–9.
126. Bora LV, Mewada RK. Visible/solar light active photocatalysts for organic effluent treatment: fundamentals, mechanisms and parametric review. Renew Sustain Energy Rev. 2017;76:1393–421.
127. Osipov AV, Tretyakov SA. Modern electromagnetic scattering theory with applications. John Wiley & Sons; 2017.
128. Hahn DW. 'Light scattering theory'. Department Mech Aerosp Eng Univ Fla, 2009;18.
129. Jagielski B. 'Elements of the wave-particle duality of light', 2009.
130. Liang Z-C. Essence of light: particle, field, and interaction. In: Photonic Fiber and Crystal Devices: Advances in Materials and Innovations in Device Applications XII. SPIE; 2018. p. 80–93.
131. Rashkovskiy SA. Quantum mechanics without quanta: the nature of the wave–particle duality of light. Quantum Studies: Math Found. 2016;3:147–60.
132. Henriksen EK, Angell C, Vistnes AI, Bungum B. What is light? Students' reflections on the wave-particle duality of light and the nature of physics. Sci Educ Dordr. 2018;27:81–111.
133. Fiorenza R, Sciré S, D'Urso L, Compagnini G, Bellardita M, Palmisano L. Efficient H2 production by photocatalytic water splitting under UV or solar light over variously modified TiO2-based catalysts. Int J Hydrogen Energy. 2019;44(29):14796–807. https://doi.org/10.1016/j.ijhydene.2019.04.035.
134. Christian GD, Dasgupta PK, Schug KA. Analytical chemistry. Wiley; 2013.
135. Tibbetts JD, Carbery DR, Emanuelsson EAC. An in-depth study of the use of Eosin Y for the solar photocatalytic oxidative coupling of benzylic amines. ACS Sustain Chem Eng. 2017;5(11):9826–35.
136. Law M, Greene LE, Johnson JC, Saykally R, Yang P. Nanowire dye-sensitized solar cells. Nat Mater. 2005;4(6):455–9.
137. Navidpour AH, Abbasi S, Li D, Mojiri A, Zhou JL. Investigation of advanced oxidation process in the presence of TiO2 semiconductor as photocatalyst: property, principle, kinetic analysis, and photocatalytic activity. Catalysts. 2023. https://doi.org/10.3390/catal13020232.
138. Anucha C, Altin I, Bacaksız E, Stathopoulos V. Titanium dioxide (TiO_2)-based photocatalyst materials activity enhancement for contaminants of emerging concern (CECs) degradation: in the light of modification strategies. Chem Eng J Adv. 2022;10:100262. https://doi.org/10.1016/j.ceja.2022.100262.
139. Díaz L, et al. M/TiO2 (M = Fe, Co, Ni, Cu, Zn) catalysts for photocatalytic hydrogen production under UV and visible light irradiation. Inorg Chem Front. 2021;8(14):3491–500. https://doi.org/10.1039/D0QI01311K.
140. Zhang D, Dai F, Zhang P, An Z, Zhao Y, Chen L. The photodegradation of methylene blue in water with PVDF/GO/ZnO composite membrane. Mater Sci Engineering: C. 2019;96:684–92.

141. Lu Y, et al. Interfacial co-existence of oxygen and titanium vacancies in nanostructured TiO2 for enhancement of carrier transport. Nanoscale. 2020;12(15):8364–70. https://doi.org/10.1039/D0NR01180K.
142. Zhang P, Wu P, Bao S, Wang Z, Tian B, Zhang J. Synthesis of sandwich-structured AgBr@Ag@TiO2 composite photocatalyst and study of its photocatalytic performance for the oxidation of benzyl alcohols to benzaldehydes. Chem Eng J. 2016;306:1151–61. https://doi.org/10.1016/j.cej.2016.08.015.
143. Gannoruwa A, Niroshan K, Ileperuma O, Bandara J. Infrared radiation active, novel nanocomposite photocatalyst for water splitting. Int J Hydrogen Energy. 2014;39:15411–5. https://doi.org/10.1016/j.ijhydene.2014.07.118.
144. Ali H, et al. A comprehensive review based on the synthesis, properties, morphology, functionalization, and potential applications of transition metals nitrides. Coord Chem Rev. 2025;526:216353. https://doi.org/10.1016/j.ccr.2024.216353.
145. Muscetta M, Clarizia L, Race M, Andreozzi R, Marotta R, Di Somma I. Visible—light driven systems: effect of the parameters affecting hydrogen production through photoreforming of organics in presence of Cu2O/TiO2 nanocomposite photocatalyst. Appl Sci. 2023. https://doi.org/10.3390/app13042337.
146. Lavand AB, Malghe YS. Visible light photocatalytic degradation of 4-chlorophenol using C/ZnO/CdS nanocomposite. J Saudi Chem Soc. 2015;19(5):471–8. https://doi.org/10.1016/j.jscs.2015.07.001.
147. Li X, et al. Temperature-induced variations in photocatalyst properties and photocatalytic hydrogen evolution: differences in UV, visible, and infrared radiation. ACS Sustainable Chemistry & Engineering. 2021;9(21):7277–85.
148. Do HH, et al. Recent progress in TiO2-based photocatalysts for hydrogen evolution reaction: a review. Arab J Chem. 2020;13(2):3653–71. https://doi.org/10.1016/j.arabjc.2019.12.012.
149. A. B. et al., 'Challenges in photocatalytic hydrogen evolution: Importance of photocatalysts and photocatalytic reactors'. Int J Hydrogen Energy, 2024;81:1442–66. https://doi.org/10.1016/j.ijhydene.2024.07.262
150. Li X, et al. Challenges of photocatalysis and their coping strategies. Chem Catal. 2022;2(6):1315–45. https://doi.org/10.1016/j.checat.2022.04.007.
151. Tahir MB, Asiri AM, Nawaz T. A perspective on the fabrication of heterogeneous photocatalysts for enhanced hydrogen production. Int J Hydrogen Energy. 2020;45(46):24544–57. https://doi.org/10.1016/j.ijhydene.2020.06.301.
152. Bie C, Wang L, Yu J. Challenges for photocatalytic overall water splitting. Chem. 2022;8(6):1567–74. https://doi.org/10.1016/j.chempr.2022.04.013.
153. He L, et al. Deep eutectic solvents for catalytic biodiesel production from liquid biomass and upgrading of solid biomass into 5-hydroxymethylfurfural. Green Chem. 2023. https://doi.org/10.1039/D3GC02816J.
154. Rahman KH, Kar AK. Influence of catalyst loading on photocatalytic degradation efficiency of CTAB-assisted TiO2 photocatalyst towards methylene blue dye solution. Bull Mater Sci. 2022;45(1):18.
155. Rajput RB, Jamble SN, Kale RB. A review on TiO2/SnO2 heterostructures as a photocatalyst for the degradation of dyes and organic pollutants. J Environ Manage. 2022;307:114533.
156. Kamble SP, Sawant SB, Pangarkar VG. Photocatalytic degradation of m-dinitrobenzene by illuminated TiO2 in a slurry photoreactor. J Chem Technol Biotechnology: Int Res Process Environ Clean Technol. 2006;81(3):365–73.
157. Kaneco S, Rahman MA, Suzuki T, Katsumata H, Ohta K. Optimization of solar photocatalytic degradation conditions of bisphenol A in water using titanium dioxide. J Photochem Photobiol A Chem. 2004;163(3):419–24.
158. Batterjee MG, Nabi A, Kamli MR, Alzahrani KA, Danish EY, Malik MA. Green hydrothermal synthesis of zinc oxide nanoparticles for UV-light-induced photocatalytic degradation of ciprofloxacin antibiotic in an aqueous environment. Catalysts. 2022;12(11):1347.
159. Aziz NA, Sheng CK. Annealing dependent morphological transition, crystallinity enhancement, IR spectra and optical properties tuning of CuO nanostructure synthesized by facile precipitation for photocatalytic applications. Rom J Phys. 2023;68:610.
160. Aziz NAB, Sheng CK. Impact of CuO loading for enhanced photocatalytic performance of CdS/CuO photocatalyst on rhodamine 6G dye decomposition under ultraviolet irradiation. Mater Lett. 2023;347:134589.
161. Neppolian B, Choi HC, Sakthivel S, Arabindoo B, Murugesan V. Solar/UV-induced photocatalytic degradation of three commercial textile dyes. J Hazard Mater. 2002;89(2–3):303–17.
162. Acar C, Dincer I, Naterer GF. Review of photocatalytic water-splitting methods for sustainable hydrogen production. Int J Energy Res. 2016;40(11):1449–73.
163. Jing D, et al. Efficient solar hydrogen production by photocatalytic water splitting: from fundamental study to pilot demonstration. Int J Hydrogen Energy. 2010;35(13):7087–97.
164. Jing D, et al. Efficient solar hydrogen production by photocatalytic water splitting: from fundamental study to pilot demonstration. Int J Hydrogen Energy. 2010;35(13):7087–97.
165. He S, Chen Y, Fang J, Liu Y, Lin Z. Optimizing photocatalysis via electron spin control. Chem Soc Rev. 2025. https://doi.org/10.1039/D4CS00317A.
166. Tuama AN, Alzubaidi LH, Jameel MH, Abass KH, Mayzan M, Salman ZN. Impact of electron–hole recombination mechanism on the photocatalytic performance of ZnO in water treatment: a review. J Sol-Gel Sci Technol. 2024;110(3):792–806.
167. Wang H, et al. Semiconductor heterojunction photocatalysts: design, construction, and photocatalytic performances. Chem Soc Rev. 2014;43(15):5234–44. https://doi.org/10.1039/c4cs00126e.
168. Zhang X, Chen YL, Liu RS, Tsai DP. Plasmonic photocatalysis. Rep Prog Phys. 2013. https://doi.org/10.1088/0034-4885/76/4/046401.
169. Atabaev TS, Molkenova A. Upconversion optical nanomaterials applied for photocatalysis and photovoltaics: recent advances and perspectives. Front Mater Sci. 2019;13(4):335–41.
170. Barros FAA, Cruz-Filho JF, Luz GE. Energy Band Engineering of Semiconductor Forward Enhanced Photocatalysis. In: Photocatalysis Approach for Environmental Applications. CRC Press; 2025. p. 94–129.
171. Zhang L, Zhang J, Yu J, García H. Charge-transfer dynamics in S-scheme photocatalyst. Nat Rev Chem. 2025(5). https://doi.org/10.1038/s41570-025-00698-3.
172. Bopape DA, Ntsendwana B, Mabasa FD. Photocatalysis as a pre-discharge treatment to improve the effect of textile dyes on human health: a critical review. Heliyon. 2024;10(20):e39316. https://doi.org/10.1016/j.heliyon.2024.e39316.
173. El Messaoudi N, et al. Advancements in adsorption and photocatalytic degradation technologies of brilliant green from water: current status, challenges, and future prospects. Mater Today Chem. 2024;42:102399. https://doi.org/10.1016/j.mtchem.2024.102399.

174. Gilani SAB, et al. pH dependent synthesis of ceria nanoparticles for efficient sunlight-driven photocatalysis of methyl orange containing wastewater. Opt Mater. 2024;148:114871. https://doi.org/10.1016/j.optmat.2024.114871.
175. Wang L, Yang T, Wei M, Guan R, Wei W, Jiang J. Machine learning and DFT dual-guidance of carbon dots implanted SrTiO3 hollow nanosphere for efficient all-pH-value photocatalysis. J Mater Sci Technol. 2025;217:169–81. https://doi.org/10.1016/j.jmst.2024.08.028.
176. Li X, Liu Y, Huang H, Cheng J. A photocatalysis-self-Fenton system based on NCDs@ZnIn2S4 composites at neutral pH and low amount of Fe2 + for the effective degradation of antibiotics. J Environ Manage. 2024;370:122580. https://doi.org/10.1016/j.jenvman.2024.122580.
177. Chen Y-W, Hsu Y-H. Effects of reaction temperature on the photocatalytic activity of TiO2 with Pd and Cu cocatalysts. Catalysts. 2021;11(8):966.
178. Mollaie F, Afroomand M, Ahmadi N, Mengelizadeh N, Balarak D. Optimization of photodegradation of acid blue 1 dye on aluminosilicate supported Cu doped TiO2 magnetic nanocatalyst using response surface methodology. Sci Rep. 2025;15(1):5550. https://doi.org/10.1038/s41598-025-89968-0.
179 Yang H, Yin C, Tan Y, Xu Y, Tang H. Anode nitrogen content estimation and purge strategy optimization of fuel cell system. Appl Energy. 2025;399:126463. https://doi.org/10.1016/j.apenergy.2025.126463.

Publisher's note